Journal of Biomolecular Structure and Dynamics

ISSN: (Print) (Online) Journal homepage: www.tandfonline.com/journals/tbsd20

New *N*-(1,3,4-thiadiazole-2-yl)acetamide derivatives as human carbonic anhydrase I and II and acetylcholinesterase inhibitors

Sam Dawbaa, Cüneyt Türkeş, Demokrat Nuha, Yeliz Demir, Asaf Evrim Evren, Leyla Yurttaş & Şükrü Beydemir

To cite this article: Sam Dawbaa, Cüneyt Türkeş, Demokrat Nuha, Yeliz Demir, Asaf Evrim Evren, Leyla Yurttaş & Şükrü Beydemir (27 Mar 2024): New *N*-(1,3,4-thiadiazole-2-yl)acetamide derivatives as human carbonic anhydrase I and II and acetylcholinesterase inhibitors, Journal of Biomolecular Structure and Dynamics, DOI: 10.1080/07391102.2024.2331085

To link to this article: https://doi.org/10.1080/07391102.2024.2331085

JOURNAL OF BIOMOLECULAR STRUCTURE AND DYNAMICS
https://doi.org/10.1080/07391102.2024.2331085

New *N*-(1,3,4-thiadiazole-2-yl)acetamide derivatives as human carbonic anhydrase I and II and acetylcholinesterase inhibitors

Sam Dawbaa[a,b,c], Cüneyt Türkeş[d], Demokrat Nuha[a,e,f], Yeliz Demir[g], Asaf Evrim Evren[a,h], Leyla Yurttaş[a] and Şükrü Beydemir[i,j]

[a]Department of Pharmaceutical Chemistry, Faculty of Pharmacy, Anadolu University, Eskişehir, Turkey; [b]Department of Doctor of Pharmacy (PharmD), Faculty of Medical Sciences, Thamar University, Dhamar, Yemen; [c]Department of Pharmacy, Faculty of Medical Sciences, Al-Hikma University, Dhamar, Yemen; [d]Department of Biochemistry, Faculty of Pharmacy, Erzincan Binali Yıldırım University, Erzincan, Turkey; [e]Department of Chemistry, Faculty of Science, Eskisehir Technical University, Eskişehir, Turkey; [f]Faculty of Pharmacy, University for Business and Technology, Prishtina, Kosovo; [g]Department of Pharmacy Services, Nihat Delibalta Göle Vocational High School, Ardahan University, Ardahan, Turkey; [h]Department of Pharmacy Services, Vocational School of Health Services, Bilecik Şeyh Edebali University, Bilecik, Turkey; [i]Department of Biochemistry, Faculty of Pharmacy, Anadolu University, Eskişehir, Turkey; [j]The Rectorate of Bilecik Seyh Edebali University, Bilecik, Turkey

Communicated by Ramaswamy H. Sarma

ABSTRACT

Various carbonic anhydrase (CA) enzyme isoforms are known today. In addition to the use of CA inhibitors as diuretics, antiepileptics and antiglaucoma agents, the inhibition of other specific isoforms of CA was reported to have clinical benefits in cancers. In this study, two groups of 1,3,4-thiadiazole derivatives were designed and synthesized to act as human CA I and II (*h*CA I and *h*CA II) inhibitors. The activities of these compounds were tested *in vitro* and evaluated *in silico* studies. The activity of the synthesized compounds was also tested against acetylcholinesterase (AChE) to evaluate the relation of the newly designed structures to the activity against AChE. The synthesized compounds were analyzed by ^{1}H NMR,^{13}C NMR and high-resolution mass spectroscopy (HRMS). The results displayed a better activity of all the synthesized compounds against *h*CA I than that of the commonly used standard drug, Acetazolamide (AAZ). The compounds also showed better activity against *h*CA II, except for compounds **5b** and **6b**. Only compounds **6a** and **6c** showed superior activity against AChE compared to the standard agent, tacrine (THA). *In silico* studies, including absorption, distribution, metabolism and excretion (ADME) and drug-likeness evaluation, molecular docking, molecular dynamic simulations (MDSs) and density functional theory (DFT) calculations, were compatible with the *in vitro* results and presented details regarding the structure–activity relationship.

Abbreviations: 1H NMR: Proton Nuclear Magnetic Resonance; 13C NMR: Carbon-13 Nuclear Magnetic Resonance; A: electron affinity; AAZ: acetazolamide; AChE: acetylcholinesterase; ADME: absorption, distribution, metabolism, excretion; Ar: aromatic; a.u.: Hartree atomic units; BBB: blood-brain barrier; brs: broad-singlet; CA: carbonic anhydrase; CAS: catalytic active site of the enzyme; ΔE: energy difference; DFT: density functional theory; DMSO: dimethyl sulfoxide; ESI: electron-spray ionization; ESP: electrostatic potential; eV: electonvolt; GI: gastrointestinal; HBA: hydrogen-bond acceptor; HBD: hydrogen-bond donor; hCA: human carbonic anhydrase; HOMO: highest occupied molecular orbital; HRMS: high-resolution mass spectroscopy; I: ionization potential; J: coupling constant; K_I: enzyme inhibition constant; Log K_p: skin permeation; Log P: lipophilicity; Log S: water solubility; LUMO: least unoccupied molecular orbital; MD: molecular docking; MDS: molecular dynamic simulations; MEP: molecular electrostatic potentials; MHz: megahertz; m.p.: melting point; η: chemical hardness; PAS: peripheral anionic site of the enzyme; PDB: Protein Data Bank; PDBID: Protein Data Bank Identifier; ppm: part per million; R^2: enzyme determination coefficient; Rg: radius of gyration; RMSD: root-mean-square deviation; RMSF: root-mean-square fluctuation; RT: room temperature; S: chemical softness; SEM: standard error of mean; SP: standard precision; TEA: triethylamine; THA: Tacrine; THF: tetrahydrofuran; TLC: thin-layer chromatography; TPSA: topological polar surface area; χ: electronegativity; μ: chemical potential; ω: electrophilicity index; μ_{tot}: total electric dipole moment

ARTICLE HISTORY
Received 19 September 2023
Accepted 11 March 2024

KEYWORDS
Carbonic anhydrase I; carbonic anhydrase II; acetylcholinesterase; 1,3,4-Thiadiazole derivatives; molecular docking; molecular dynamic simulations

1. Introduction

Many proteins are called metalloproteins because they need metal ions to function correctly (Gregory et al., 1993). In metalloproteins, metal ions typically play one of two major structural or functional roles. These ions either help accomplish a wide range of biological functions of the protein by directly participating in chemical catalysis or by maintaining

CONTACT Sam Dawbaa sdawbaa@tu.edu.ye, dawbaa655@anadolu.edu.tr, Sdoubaa@yahoo.com Department of Doctor of Pharmacy (PharmD), Faculty of Medical Sciences, Thamar University, Dhamar 87246, Yemen.

Supplemental data for this article can be accessed online at https://doi.org/10.1080/07391102.2024.2331085.

protein structure and stability (Dokmanić et al., 2008). Metalloenzymes play a key role in numerous crucial biological processes, such as protein degradation and nucleic acid modification (Chen et al., 2018). This case may be caused by an endogenous metalloenzyme's overexpression, increased activation or improper control. Due to their function in these processes, metalloenzymes are also crucial for developing many diseases, making them appealing candidates for therapeutic intervention (Yang et al., 2016). Their importance as a class of targets and their role in disease progression has increased awareness of their significance, stoking interest in innovative approaches to developing inhibitors and, ultimately, valuable medications.

The first metalloenzymes described concerning zinc ions were carbonic anhydrases (CAs; EC 4.2.1.1). To create the bicarbonate anion, CAs help to hydrate carbon dioxide reversibly (Nocentini et al., 2021). Many biological activities, including controlling the pH and CO_2 levels in the blood, depend on this response (Thiry et al., 2008). Inhibitors of human (*h*) CAs (*h*CAIs), the oldest known zinc ion-dependent metalloenzyme, have long been investigated as potential diuretics and anticancer drugs (Supuran & Scozzafava, 2000b). With 20 FDA-approved *h*CAIs known to date, glaucoma therapy is where *h*CAIs are most commonly used (Long et al., 2013). A wide variety of organisms include CAs, with mammals being the only group that contains the α-CA type. *h*CA II is a monomeric metalloenzyme that is 29 kDa in size and serves as a standard example (Bulos et al., 2021). A twisted β-sheet in the *h*CA II's center roughly divides the enzyme. Its active site is divided into two parts, one of which is a hydrophobic wall, and the other is an organized water network (Alterio et al., 2012). The catalytic zinc-ion for *h*CA II is located at the bottom of a 15 Å deep gap, where it is tetrahedrally bound by three histidine residues (His94, His96 and His119) and a water molecule (Aouad et al., 2022). Additionally, the catalytic activity of its nearby Thr199 residue and the metal-bound water is stabilized by a hydrogen bond (Di Fiore et al., 2022).

This study was achieved to examine the potency and selectivity of newly designed inhibitors of some *h*CA isoforms. Hence, we focused on the first-generation CA inhibitor Acetazolamide (AAZ), a drug molecule that is in clinical use mainly due to its diuretic, antiglaucoma and antiepileptic effects (Supuran & Clare, 1999; Supuran & Scozzafava, 2000a). By keeping the amide and thiadiazole parts of the drug, named *N*-(5-sulfamoyl-1,3,4-thiadiazole-2-yl)acetamide, phenyl aminoacyl (**5a**–**5d**) and phenyl acyl (**6a**–**6d**) derivatives connected by a thioether bridge were obtained (Figure 1). In medicinal chemistry, 1,3,4-thiadiazole derivatives are known primarily for their diuretic (Ergena et al., 2022) and antiglaucoma activities (Kasımoğulları et al., 2010). Additionally, their anticancer (Abas et al., 2021), antibacterial (Wu et al., 2021), antifungal (Karaburun et al., 2018), antioxidant (Gowda et al., 2020), anticholinesterase activities (Lotfi et al., 2020; Skrzypek et al., 2021) and CA inhibitory (Abdel-Hamid et al., 2007) properties were reported. The 1,3,4-thiadiazole ring is preferred chemically for the synthesis of new drug candidates due to its liposolubility and mesoionic structure (Fu et al., 2016), as well as being more susceptible to nucleophilic attacks (C-2, C-5) (Atmaram & Roopan, 2022). On the other hand, since the nitrogen-containing functional groups with increased nucleophilic power as in the sulfonamide structure are known to coordinate with zinc in CAs, the sulfur atom with higher nucleophilic power can be coordinated with zinc both by being directly attached to the ring and by the acyl group on the other side. Thus, by replacing this group with the thioether group, it is thought that the CA inhibitory activity may be at the same level or higher.

In this study, we aimed to design and synthesize small molecules with high CA inhibitory effect by focusing on a prominent drug, AAZ. The designed 1,3,4-thiadiazole derivatives were synthesized and analyzed using various spectroscopic methods. The inhibitory action of the target compounds was then tested toward *h*CA isoforms I and II and acetylcholinesterase (AChE). Additionally, molecular docking studies of these derivatives were conducted to study

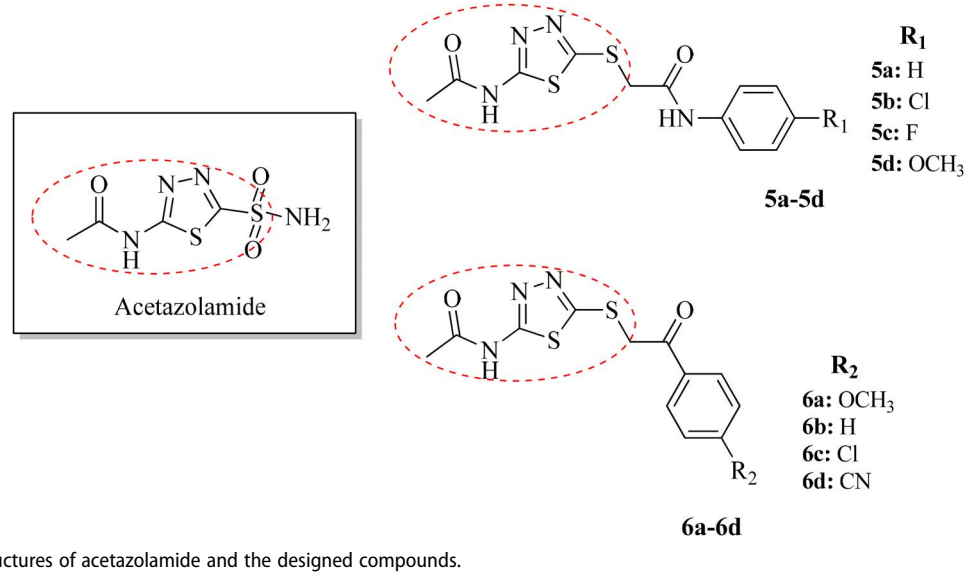

Figure 1. Chemical structures of acetazolamide and the designed compounds.

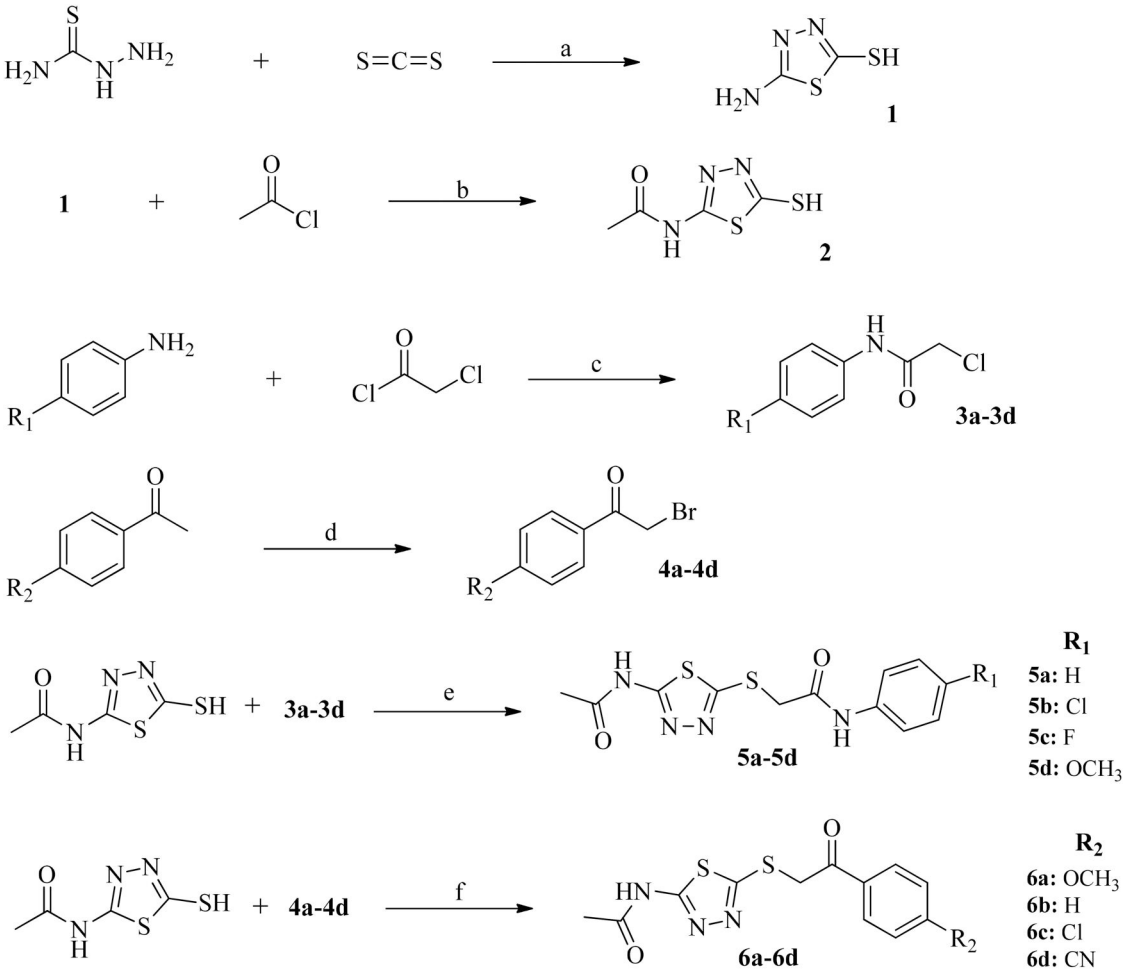

Scheme 1. The synthesis diagram of the compounds **5a–5d** and **6a–6d**. Reagents and conditions: (a) Na_2CO_3, EtOH, reflux, 4 h; (b) Triethylamine (TEA), THF, 0 °C, 2 h; (c) TEA, THF, 0 °C, then stirring at RT for 5 h; (d) HBr, Br_2, Acetic acid, 0–5 °C, then stirring at RT for 3 h; (e) K_2CO_3, Acetone, stirring at RT for 24 h; (g) K_2CO_3, Acetone, stirring at RT for 24 h.

the expected *in silico* binding modes of the newly synthesized derivatives in the *h*CAs, and AChE active sites.

2. Results and discussion

2.1. Chemistry

In this study, eight novel 2,5-disubstituted 1,3,4-thiadiazole derivatives (**5a–5d, 6a–6d**) were designed and synthesized as shown in Scheme 1. In the synthesis step, 5-amino-1,3,4-thiadiazole-2-thiol (**1**) was obtained by reacting thiosemicarbazide with carbon disulfide. Acetylation of the amino group of this compound with acetyl chloride formed the acyl derivative *N*-(5-mercapto-1,3,4-thiadiazole-2-yl)acetamide (**2**). Other starting materials were synthesized by acetylation of various aniline derivatives (**3a–3d**) using 2-chloroacetyl chloride and bromination of acetophenone derivatives (**4a–4d**). Reacting compounds **3a–3d** and **4a–4d** with compound **2** resulted in 2-((5-acetamido-1,3,4-thiadiazole-2-yl)thio)-*N*-phenylacetamide derivatives (**5a–5d**) and *N*-(5-((2-oxo-2-phenylethyl)thio)-1,3,4-thiadiazole-2-yl)acetamide derivatives (**6a–6d**), respectively. The yields ranged between 71% and 89%.

The structures of the synthesized compounds **5a–5d** and **6a–6d** were confirmed by ^{1}H-NMR, ^{13}C-NMR and high-resolution mass spectroscopy (HRMS). The chemical structures of the final compounds differ due to the amino function attached to the phenyl ring. In the ^{1}H-NMR spectra of the compounds, the hydrogen attached to this amino nitrogen atom is observed between 10.21 and 10.50 ppm; the other N-H resonates around 12.59 ppm as broad singlets. In compounds **5a–5d**, the methylene proton (NHCO$\underline{CH_2}$) was found to be between 4.16 and 4.21 ppm. The signals of $COCH_2$ in the other derivatives **6a–6d** were detected between 4.98 and 5.05 ppm. The characteristic two symmetrical doublets in the aromatic region were assigned the *para*-disubstituted phenyl moiety.

In the ^{13}C-NMR spectra, the carbon signal of the CH_3 belonging to the acetamide residue attached to the thiadiazole ring was observed between 22.25 and 23.75 ppm, while the carbon signal of the CO was detected between 169.21 and 169.23 ppm. The carbon signals belonging to the S-CH_2-CO group, on the other hand, were detected between 38.32 and 41.78 ppm for CH_2 and around 165.39–167.76 ppm for CO. The carbon signal of the carbonyl group in the **6a–6d** compounds shifted downfield compared to the **5a–5d** compounds and was observed around 191.72–193.54 ppm. In the HRMS spectra, $M + 1$ peaks were observed in agreement with the calculated molecular weights of compounds **5a–5d** and **6a–6d** in positive ion mode.

Table 1. Inhibition data of *h*CA isoforms and AChE with novel synthesized 1,3,4-thiadiazole derivatives (**5a–5d** and **6a–6d**) and the reference inhibitors acetazolamide and tacrine, the clinically used drug.

	*h*CA I			*h*CA II			AChE		
Compounds	K_I[a] (nM)	R^2	Inhibition type	K_I[a] (nM)	R^2	Inhibition type	K_I[a](nM)	R^2	Inhibition type
5a	76.48 ± 8.91	0.9826	Competitive	54.81 ± 6.07	0.9845	Competitive	213.00 ± 19.51	0.9887	Competitive
5b	133.80 ± 10.41	0.9850	Noncompetitive	193.60 ± 17.48	0.9860	Noncompetitive	186.60 ± 19.34	0.9864	Competitive
5c	120.70 ± 12.73	0.9873	Competitive	95.23 ± 11.44	0.9836	Competitive	285.70 ± 28.06	0.9874	Competitive
5d	139.80 ± 17.06	0.9825	Competitive	118.30 ± 13.41	0.9860	Competitive	177.90 ± 16.38	0.9883	Competitive
6a	77.49 ± 8.63	0.9841	Competitive	64.22 ± 6.99	0.9848	Competitive	78.26 ± 7.46	0.9857	Competitive
6b	216.30 ± 29.88	0.9831	Competitive	283.80 ± 21.83	0.9866	Noncompetitive	240.40 ± 17.09	0.9834	Noncompetitive
6c	121.10 ± 14.45	0.9862	Competitive	61.28 ± 6.53	0.9874	Competitive	132.30 ± 12.68	0.9869	Competitive
6d	79.70 ± 10.06	0.9830	Competitive	52.90 ± 5.58	0.9875	Competitive	178.30 ± 17.89	0.9866	Competitive
AAZ[b]	454.10 ± 25.57	0.9869	Noncompetitive	157.80 ± 15.33	0.9860	Noncompetitive	–	–	–
THA[c]	–	–	–	–	–	–	164.80 ± 13.55	0.9873	Competitive

[a]The test results were expressed as means of triplicate assays ± SEM, [b]Acetazolamide and [c]Tacrine.

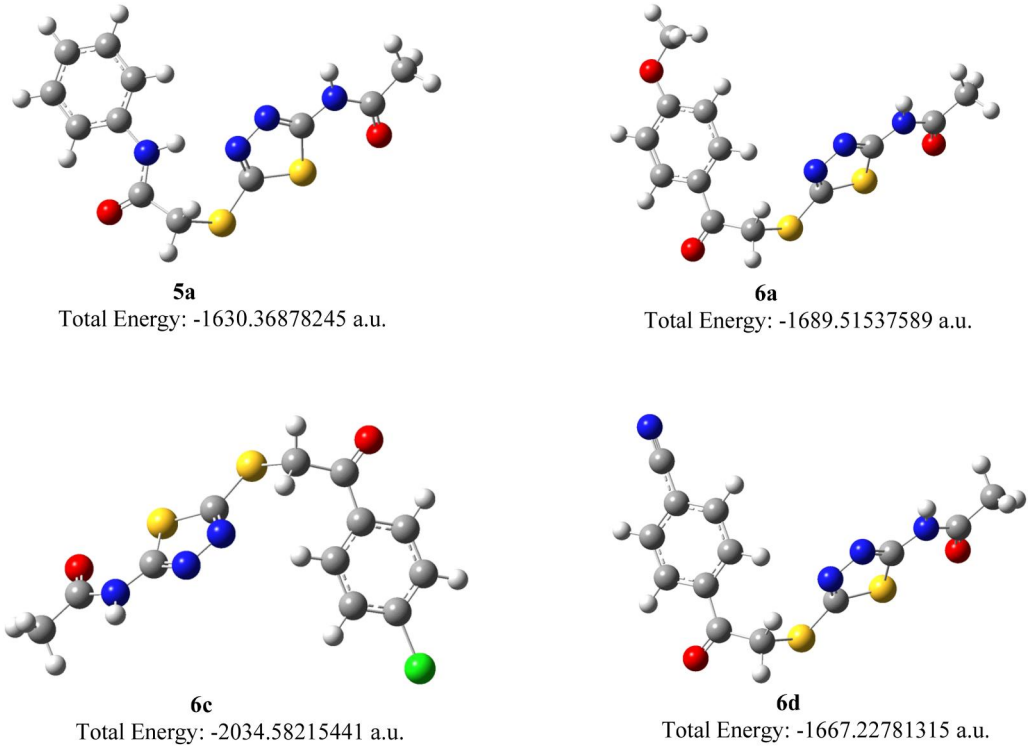

Figure 2. Optimized molecular structures and total energy values of the active compounds.

2.2. h*CA and AChE inhibitory activity of the target compounds*

Using the esterase assay in accordance with Verpoorte's technique, the target 1,3,4-thiadiazole derivatives **5a–5d** and **6a–6d** were tested for their ability to inhibit the physiologically and pharmacologically relevant cytosolic *h*CA I, II and AChE. AAZ and tacrine (THA) were employed in the analyses as conventional inhibitors because they are medications often prescribed. Table 1 summarizes the enzyme inhibition constants (K_I) and their coefficient of determination (R^2).

The cytosolic isoform *h*CA I was potently inhibited by 1,3,4-thiadiazole derivatives (**5a–5d** and **6a–6d)** with K_Is in the low nanomolar range of 76.48 ± 8.91 – 216.30 ± 29.88 nM, indicating that all synthesized compounds are more potent inhibitors than the reference drug AAZ (K_I of 454.10 ± 25.57). The most active derivatives in this series are compounds **5a**, **6a** and **6d**, which have K_Is of 76.48 ± 8.91 nM, 77.49 ± 8.63 nM and 79.70 ± 10.06 nM, respectively, whilst the weakest inhibitor in this group, compound **6b**, which has a K_I of 216.30 ± 29.88 nM.

Exploring the inhibitory effect of the herein reported 1,3,4-thiadiazole derivatives (**5a–5d** and **6a–6d)**, all molecules (except **5b** and **6b** with K_Is of 193.60 ± 17.48 nM and 283.80 ± 21.83 nM, respectively) showed potent inhibitory action toward the physiologically dominant *h*CA II isoform with K_Is ranging from 52.90 ± 5.58 nM to 118.30 ± 13.41 nM, which is even better than the standard drug AAZ (K_I of 157.80 ± 15.33 nM). In particular, compound **6d** exhibited the best *h*CA II inhibitory effect with two-digit nanomolar activity (K_I of 52.90 ± 5.58 nM). Also, compounds **5a** and **6c** had a potent *h*CA II inhibitory effect with two-digit nanomolar activities (K_Is of 54.81 ± 6.07 nM and 61.28 ± 6.53 nM, respectively).

All the synthesized **5a–5d** and **6a–6d** derivatives inhibited the AChE, with two or three-digit K_Is of 78.26 ± 7.46 nM to

285.70 ± 28.06 nM. Compounds **6a** and **6c** showed robust inhibitory effects with K_Is of 78.26 ± 7.46 nM and 132.30 ± 12.68 nM, respectively, compared to the standard drug THA (K_I of 164.80 ± 13.55 nM). Also, compound **5d** (K_I of 177.90 ± 16.38 nM) displayed equipotent activity relative to compound **6d** (K_I of 178.30 ± 17.89 nM). Conversely, compound **5c** (K_I of 285.70 ± 28.06 nM) recorded the least inhibiting effect in the group.

2.3. Results of DFT studies

2.3.1. The theoretical geometry analysis and dipole moments

The findings of optimizing the molecular structures with total energy values of the active compounds using DFT/B3LYP/6-31G (d, p) are displayed in Figure 2. The total energy values for the most active chemicals are listed in the following order: **6c** < **6a** < **6d** < **5a**. Substances with lower total energy values have a more stable structure.

Calculations regarding the dipole moment were achieved to understand more about the polarity of the molecules. Thus, using Equation (1), the dipole moment was computed at the DFT/B3LYP/6-31G (d, p) level, and the results are presented in Table 2. The results suggest that compound **6a** is more polar, whereas molecule **6c** has less polarity in comparison.

2.3.2. Frontier molecular orbitals

HOMO–LUMO energy values (frontier molecular orbital energies) are important in determining some reactivity features of respective substituents of the studied molecules. Nucleophilicity and electrophilicity can be indicated by such studies as high HOMO and low LUMO energies show the ability of a molecule to donate or accept electrons, respectively (Fukui, 1982). In addition, the energy gap (HOMO–LUMO, ΔE) provides details about the molecular reactivity and stability. The narrower the energy gap, the less stable and more reactive the molecule. The active compounds' HOMO, LUMO and ΔE values are shown in Table 3. The results show that compound **6d** has the smallest ΔE measuring at 0.1470 eV, whereas compound **6a** has the largest ΔE measuring at 0.1701 eV. This data suggest that compound **6d** is less stable and more reactive than the other compounds. Figure 3 depicts the active compounds' HOMO–LUMO orbital diagrams.

The results showed that compound **5a** has a low ionization potential (*I*) and compound **6d** has a high electron affinity (*A*). This indicates that compound **6d** has electrophilic properties, in contrast to compound **5a** which has nucleophilic properties. On the other hand, the electronegative properties (χ) of the target compounds were evaluated. The descending order of compounds with χ is **6d** > **6c** > **6a** > **5a,** and the order regarding ω values is the same. As can be shown, compound **6d** has a higher electronegativity (0.1638 eV) and a more electrophilic power (0.1825 eV) than the others. Whereas, the chemical hardness (η)-softness (S) characteristics of compound **6a** were assigned by higher S and lower η values, which are beneficial in evaluating the intramolecular charge transfer.

2.3.3. Evaluation of molecular electrostatic potentials (MEP) values

The force acting on a positive test charge (a proton) positioned at a specific location (p, in the vicinity of a molecule) through the electrical charge cloud produced by the molecule's electrons and nuclei is known as the molecular electrostatic potential (MEP) at that specific location p(x,y,z). MEP is an effective indicator of the reactivity of molecules toward variously charged reactants (no polarization occurs) even when the external test charge does not affect the charge distribution (Politzer & Murray, 2002). According to the MEP scheme, red denotes a partial negative charge due to an electron-rich zone; blue denotes a partial positive charge due to an electron-deficient zone; yellow denotes a moderately electron-rich zone; and green denotes a neutral zone (Luque et al., 1993). The MEP of the active substances is depicted in Figure 4.

2.4. Molecular docking and molecular dynamic simulations studies

2.4.1. AChE enzyme inhibition and SAR

Compounds **6a** and **6c** were investigated for their behavior in the enzyme's active pocket. The stability of the ligand-protein complex was evaluated by molecular docking and molecular dynamic simulation (MDS) studies. According to the molecular docking studies, hydrophobic moieties of both compounds faced and interacted with Trp86 amino acid (of catalytic active site-CAS region). The acetamide functional groups were positioned on the entrance cavity of the active region which is surrounded by Ser203 and Trp286 residues. Both ligands **6a** and **6c** did not connect with Ser203 and Trp286 residues. However, compound **6a** interacted with Tyr124 (π–π interaction and H-bond), Phe295 (H-bond), Arg

Table 2. The values of electric dipole moment of the active compounds.

Compounds	μ_x (Debye)	μ_y (Debye)	μ_z (Debye)	μ_{tot} (Debye)
5a	5.5100	3.8130	1.8903	6.9622
6a	3.7045	6.1917	2.0399	7.4981
6c	4.1436	3.1561	1.8784	5.5370
6d	5.5105	0.3569	2.1174	5.9141

Table 3. Some reactivity parameters of the active compounds.

Compounds	E_{HOMO} (eV)	E_{LUMO} (eV)	ΔE (eV)	*I* (eV)	*A* (eV)	χ (eV)	η (eV)	S (eV^{-1})	μ (eV)	ω (eV)
5a	−0.2113	−0.0542	0.1571	0.2113	0.0542	0.1327	0.0785	6.3654	−0.1327	0.1121
6a	−0.2240	−0.0539	0.1701	0.2240	0.0539	0.1389	0.0850	5.8823	−0.1389	0.1134
6c	−0.2319	−0.0706	0.1613	0.2319	0.0706	0.1512	0.0806	6.2035	−0.1512	0.1417
6d	−0.2373	−0.0903	0.1470	0.2373	0.0903	0.1638	0.0735	6.8027	−0.1638	0.1825

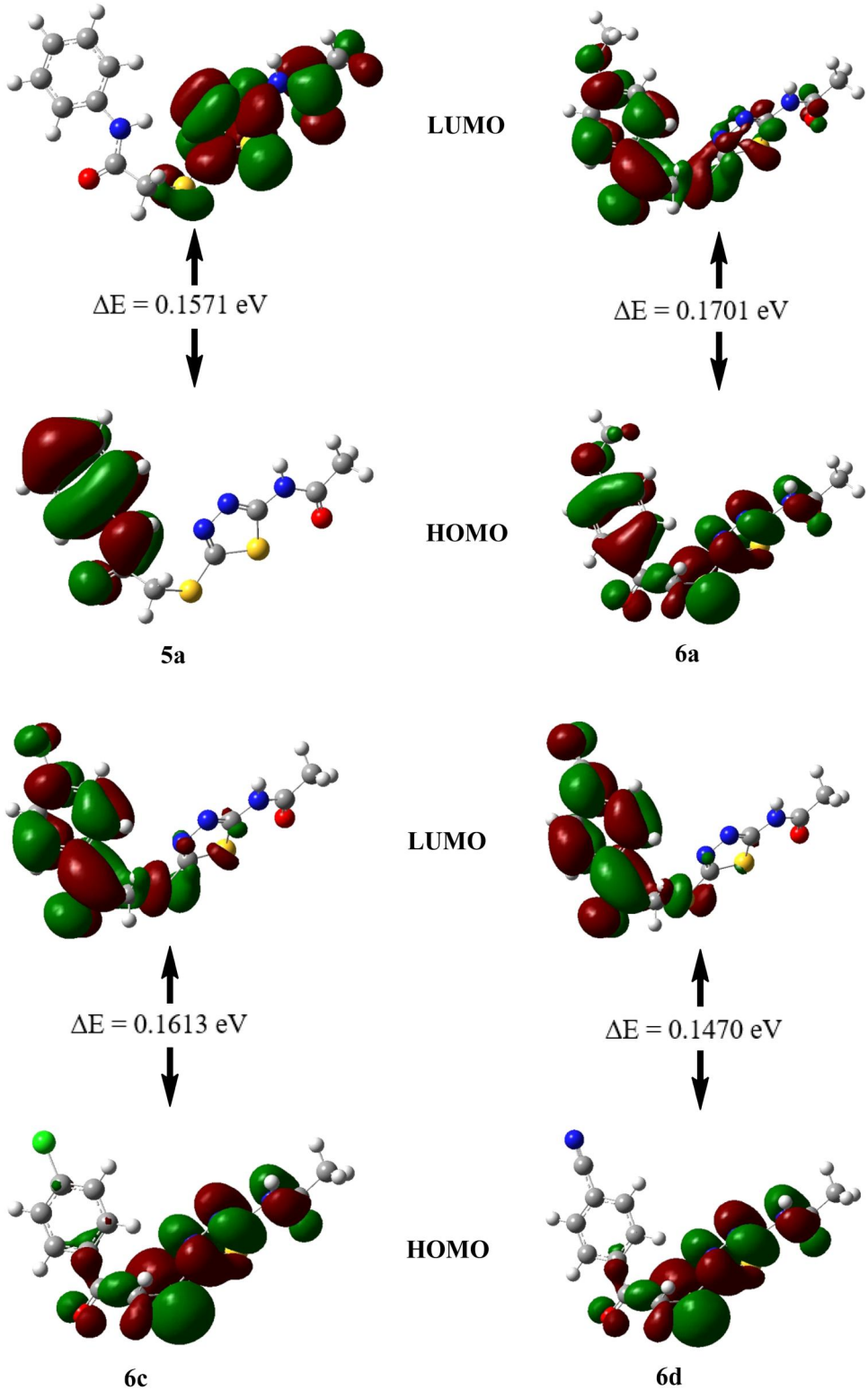

Figure 3. HOMO–LUMO diagrams of the active compounds.

(H-bond), Tyr337 (Ar H-bond) and His447 (π–π interaction). On the other hand, compound **6c** interacted with Glh202 (Ar H-bond), Phe297 (Ar H-bond), Tyr337 (Ar H-bond), Phe338 (Ar H-bond) and Tyr341 (π–π interaction). To increase the inhibitory activity, we think a bulkier group such as phenyl- or heteroaryl-acetamide had to replace the acetamide group. The molecular docking results are illustrated in Figure 5.

According to certain studies (Coşkun et al., 2023; Osmaniye, Evren, et al., 2022; Turan Yücel et al., 2022), the stability properties of the complex should be explained before discussing the binding mode results of MDSs. In this study, the alteration of radius of gyration (Rg) values was presented in Figure 6(A) and the changing of these values was observed between 3.9 and 4.8 Å. Our root-mean-square

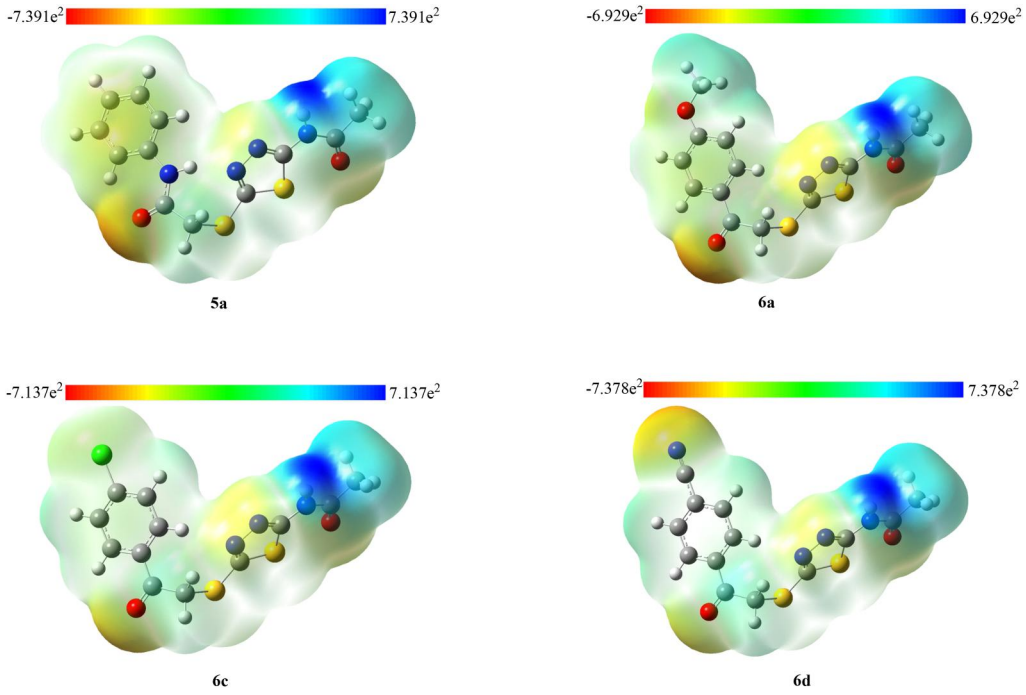

Figure 4. Molecular electrostatic potential (MEP) surfaces of the active compounds. The electrostatic potential (ESP) is given in Hartree atomic units (a.u.).

deviation (RMSD) values of ligand fit on protein, ligand fit on ligand and enzyme protein were 0–4.20 Å, 0–1.92 Å and 0–1.82 Å, respectively (Figure 6(B)). Moreover, root-mean-square fluctuation (RMSF) analysis indicated that the RMSF values of α-helix and the β-sheet amino acid residues did not show drastic changes during the simulation (Figure 6(C)). Additionally, interacted loop amino acids were calculated under 0.8 Å. All these findings support that stability was evidenced during the entire simulation, thus, the results of the reported interactions are trustable.

MDS study revealed that the 4-methoxy phenacyl group is an essential residue for the interaction with CAS pocket residues (Trp86 and Gly120). Moreover, even though π–π interaction with Trp286 could not be observed after 20 ns in the simulation as was observed in the docking findings, it did not affect the stability of the complex. But to protect the stability, compound **6a** slightly moved from Trp286 to interact with Arg493 at the PAS region. Similar to the natural substrate of the AChE enzyme (acetylcholine), the acetamide moiety of compound **6a** is located in the same esteric site as acetylcholine (Dvir et al., 2010), but there is no interaction with Ser203 or Trp286 residues. This might be caused by the affinity of the acidic nitrogen of compound **6a** toward Tyr124 residue, which causes a change in the pose at the PAS region (see Figure 6(B) and around 20 ns of the **video**). Arg493 residue is known to penetrate the active-site gorge and stacks against Trp286 residue (PAS amino acid). Therefore, this and other residues within the PAS that may participate in the interaction with this loop (like the Tyr124 residue) enhance the inhibition activity. Hence, compound **6a** formed an H-bond and a water-mediated H-bond with Tyr124 and made some hydrophobic interactions too. Although a lack of direct interaction with Trp286 was observed, the relationship with Tyr124 amino acid clarified how the enzyme can be inhibited by explaining the binding mechanism of the PAS region. Furthermore, compound **6a** also interacted with Phe295, Tyr337, Phe338 and Ser125 amino acids. All of these residues increased the complex's stability, which in turn increased compound **6a**'s inhibitory activity. In conclusion, the inhibitory activity of compound **6a** is based on the interactions with Trp86, Glu120 and Tyr124 residues. Thus, the 4-methoxyphenyl and acetamide moieties are thought to be essential for the anti-AChE activity.

2.4.2. h*CA I enzyme inhibition and SAR*

Molecular docking and MDSs studies were used to understand the behavioral profile of ligands and proteins together. According to molecular docking studies, the acetamide moiety of the compounds **5a**, **6a** and **6d** interacts with the zinc atom (Zn301) *via* a salt bridge and/or metal chelation. The sulfanilamide moiety, which is more acidic than the acetamide of AAZ, has an affinity for the divalent metal atom (Zn^{2+}), while the acetamide of AAZ is positioned in the entrance cavity of the enzyme. Similar to AAZ, the acetamide moiety is more acidic than the aryl group of the synthesized compounds and is chelated with a Zn^{2+} ion in the active pocket of the enzyme. On the other hand, the hydrophobic group of the most active compound interacted with His64 and His200 amino acids.

While the methoxy group of compound **6a** was verging to some positively charged amino acids, the cyano group of compound **6d** faced some polar uncharged residues (blue and cyan colored in Figure 7(A)). The acyl derivative **5a** interacted similarly to compound **6a** with some polar, uncharged residues. This orientation affected the interaction with His200, where the hydrophobic group of compound **5a** was expected to interact with His200 by π–π stacking while that

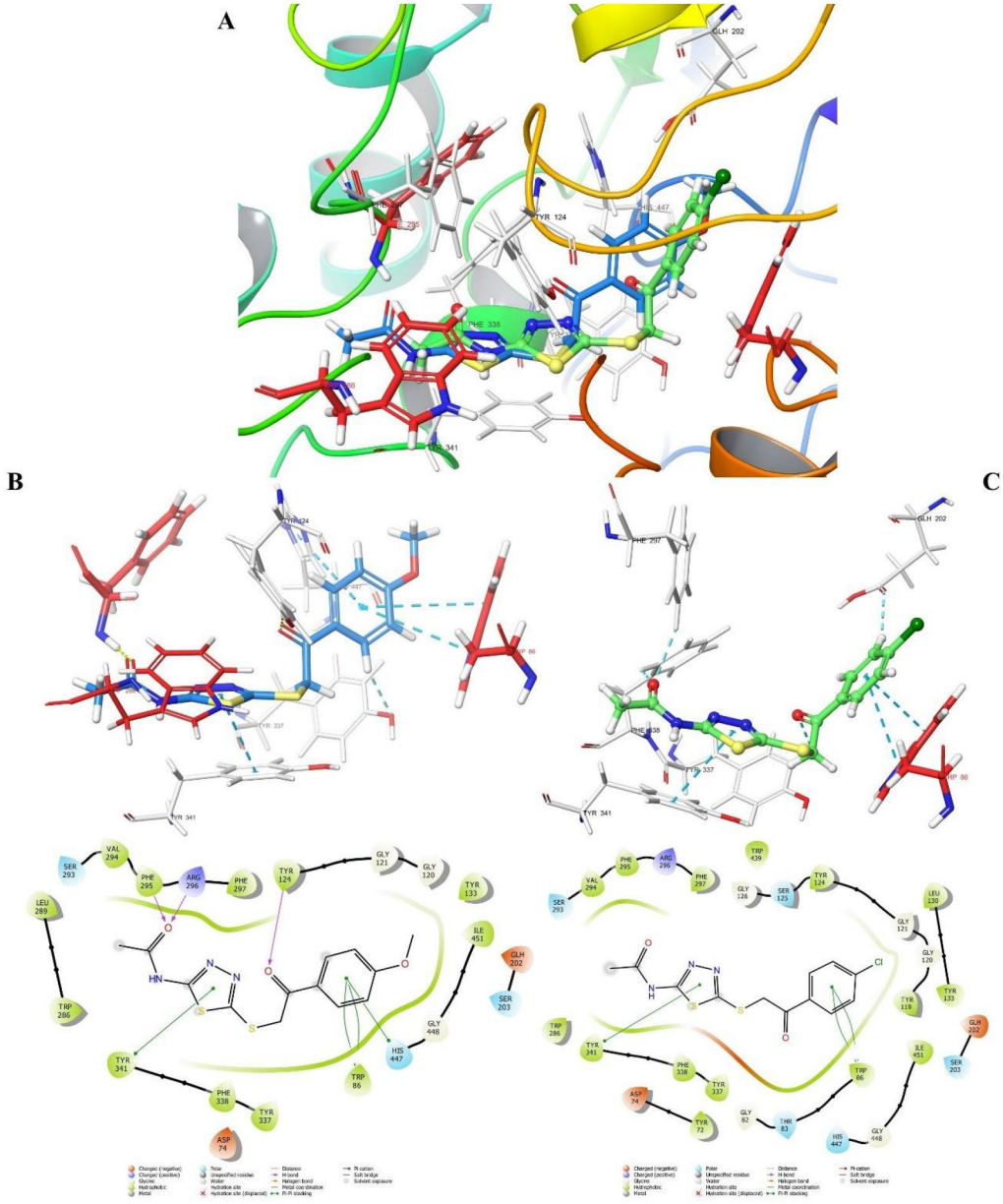

Figure 5. 2D and 3D Docking poses of compounds **6a** and **6c** in the active site of AChE enzyme (PDBID: 4EY7). (A: Superimposition of the compounds **6a** & **6c**; B: Compound **6a**; C: Compound **6c**).

of compound **6d** could not reach His200. This is explained by the effect of the extra N atom (as an elongation scaffold) in compound **5a'**s side chain, which is absent in compound **6d**. Indeed, the hydrophobic moiety of compound **5a** did not show any affinity for His200, while the acetamide nitrogen of compound **6a** formed an H-bond with His200. This pose of compound **6a** affected the interaction between His94 and the thiadiazole ring of the ligand, thus compound **6a** could not face His94 residue.

Regarding the acetyl group, some interaction was observed with His67, while the acyl group could not interact with this amino acid. The amino acid sequence number 67 is different between all CA isoforms (Güzel-Akdemir et al., 2015). *h*CA I and *h*CA II have His67 and Asn67, respectively; and His67 is bulkier than Asn67. So, the entrance cavity of the *h*CA I enzyme is smaller than that of the *h*CA II enzyme. Thus, compounds that have lipophilic or bulky groups localize in the *h*CA II cavity better than the *h*CA I cavity. For this reason, our results showed that compound **6c** which has a 4-chlorophenyl group, caused a more inhibitory effect on the *h*CA II than that on the *h*CA I enzyme. Accordingly, two acetamide groups on C-2 and C-5 of the thiadiazole ring with no substitutions on the aromatic ring are thought to be preferable to get *h*CA I inhibition activity and/or *h*CA I inhibition selectivity. In the case of the presence of one acyl moiety and one acetamide moiety on the thiadiazole ring, the substitution on the aromatic ring should be modified with a small hydrophobic group to set the lipophilicity of the molecules.

According to the MDS study on the **5a**-*h*CA I complex (Figure 8), the stability indicators Rg, RMSD and RMSF were evaluated. The Rg plot did not show drastic changes, and the value changes are observed between 3.5 and 4.5 Å similar to that of the **6c**-AChE enzyme complex. Our RMSD diagram indicated that the values of ligand fit on protein, ligand fit on ligand and

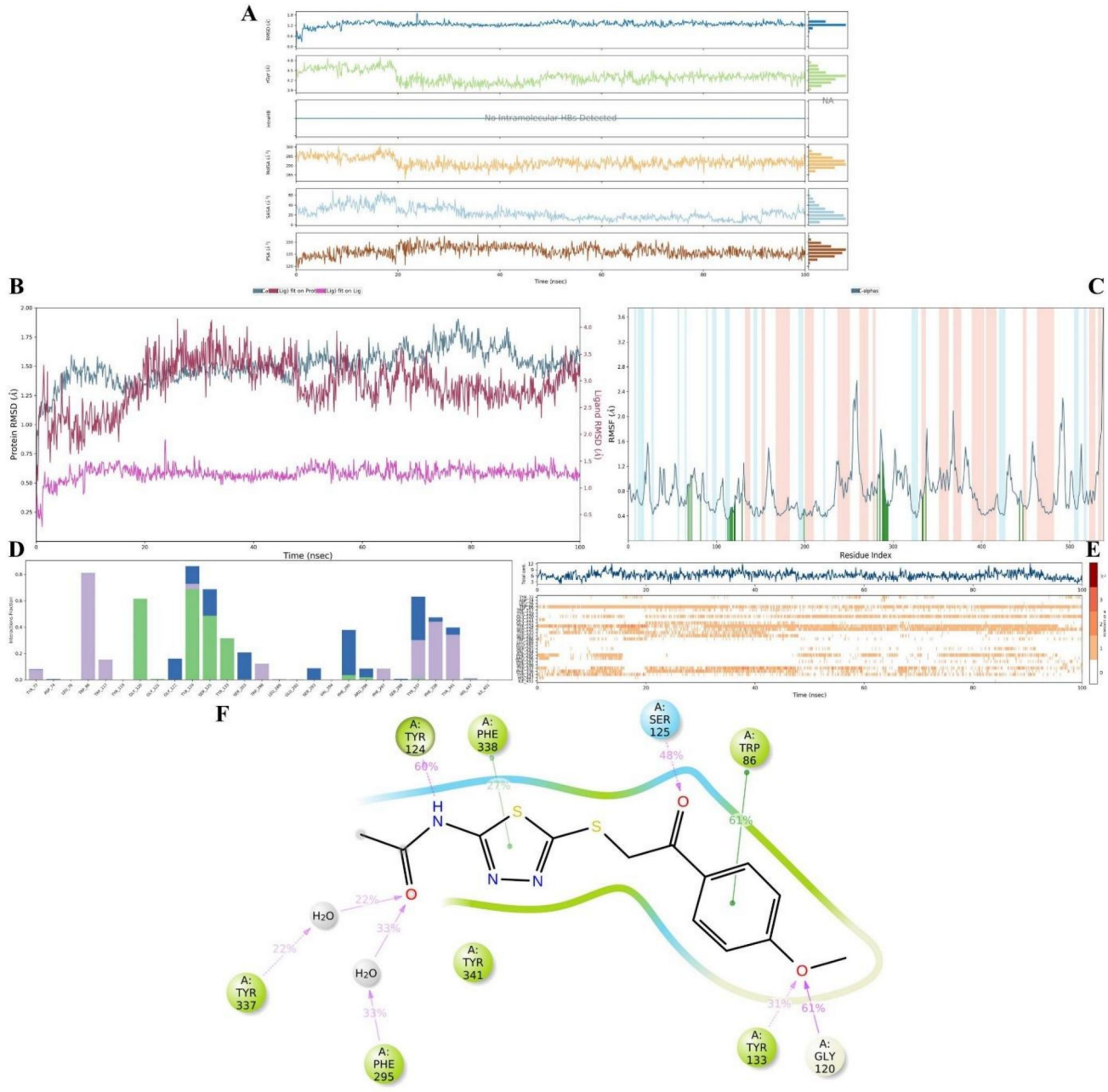

Figure 6. Plots of the MDS results for **6a**-AChE enzyme complex. Figures A–C illustrate the stability properties Rg, RMSD and RMSF, respectively; The interaction properties are illustrated in D: Interaction fraction-residue diagram, E: Total connection residues-time plot, F: 2D interaction pose with connection strength (cut off = 0.2) at the active region.

enzyme protein properties were determined in the ranges 0–5.82, 0–2.67 and 0–1.72 Å, respectively.

The chelation between acetamide and divalent metal atom (Zn^{2+}) has a significant impact on the inhibition activity. Therefore, the acetamide group is marked as an essential pharmacophore unit for the designed compounds. On the other hand, the substitutions on the C-5 of the thiadiazole ring affected not only the physicochemical parameters but also the approach of binding of the ligand to the enzyme as previously mentioned in the docking results. The pattern ligand **5a** interacted *via* chelation and H-bonds with the enzyme residues. The H-bonds were formed directly with Tyr199 and His200 after breaking the intramolecular H bond. Even though this intramolecular H-bond breaking affected its own RMSD values negatively, it held the protein's RMSD optimally, which caused the protection of the complex stability *via* the binding with Tyr199 and His200 residues.

During the whole simulation, the metal-binding histidine residues (His94, His96 and His119) and the acetamide oxygen of the ligand were chelated to the zinc ion simultaneously. This connection is essential to the inhibition of metal-dependent enzymes such as *h*CA. As a result, *in vitro* findings and *in silico* results are compatible with each other.

2.4.3. h*CAII enzyme inhibition and SAR*

The four most active compounds, **5a**, **6a, 6c** and **6d**, were docked into the cone-shaped cavity of the *h*CA II enzyme.

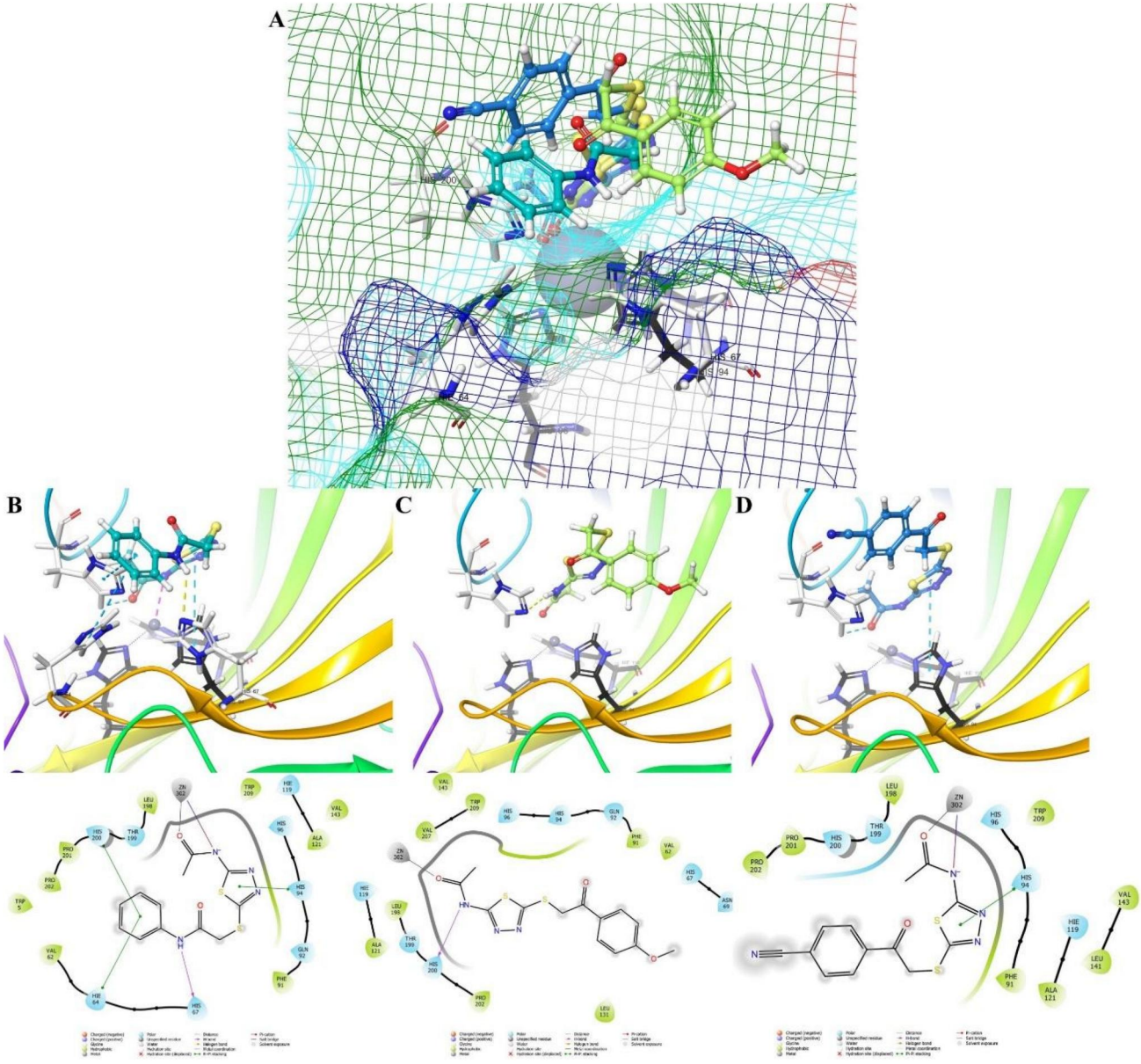

Figure 7. 2D and 3D Docking poses of compounds **5a**, **6a** and **6d** in the active site of the *h*CA I enzyme (PDBID: 2NMX). A: Superimposition of the compounds at the active pocket mapped by residue type; B: Compound **5a**; C: Compound **6a**; D: Compound **6d**).

The findings point out that the acetamide moieties of the compounds built salt bridges with the Zn metal ion of the enzyme, which is an essential binding for metal-dependent enzyme inhibition. Lipophilic groups such as Cl on the phenyl ring were observed canalizing their ligand tail into the hydrophobic region of the enzyme surface. In contrast, the hydrophilic groups such as methoxy and cyano groups (which can form H-bonds) directed themselves toward polar, uncharged residues (cyan mapping in Figure 9(A)). We found that the small activity differences are mostly related to this orientation. For this reason, we suggested newly designed molecules that include hydrophilic and potential H-bond acceptors such as nitro and ethoxy groups which are thought to increase the inhibition activity. These ideas are still on paper, and they are planned to be tested.

As mentioned in the *h*CA I docking paragraph, sequence 67, (for *h*CA II, it's Asn67), is responsible for *h*CA II selectivity. Compounds **5a**, **6a** and **6c** interacted with this residue, and compounds **5a** and **6d** interacted with the Phe131 amino acid. The importance of this residue results from its construction in one of the α-helix regions (seq. no: 131-134), and this α-helix lies near the entrance cavity to face up Asn67. Hence, maintaining this contact also means inhibiting enzyme activity. Generally, the docking study showed that the most active compounds commonly interact with Zn^{2+} and Tyr199. Besides that, they also interacted with either Asn67 or Phe131. However, the inhibitory effect is based on blocking Zn^{2+} and Tyr199 as mentioned in previous studies (Kakakhan et al., 2023; Kalinin et al., 2022).

An important consideration is that the central aromatic ring should be substituted with a small acidic group such as the acetamide moiety to allow the ligand to reach the zinc metal and its surrounding residues at the cone-shaped cavity. The interaction with the peripheral amino acids of the entrance cavity

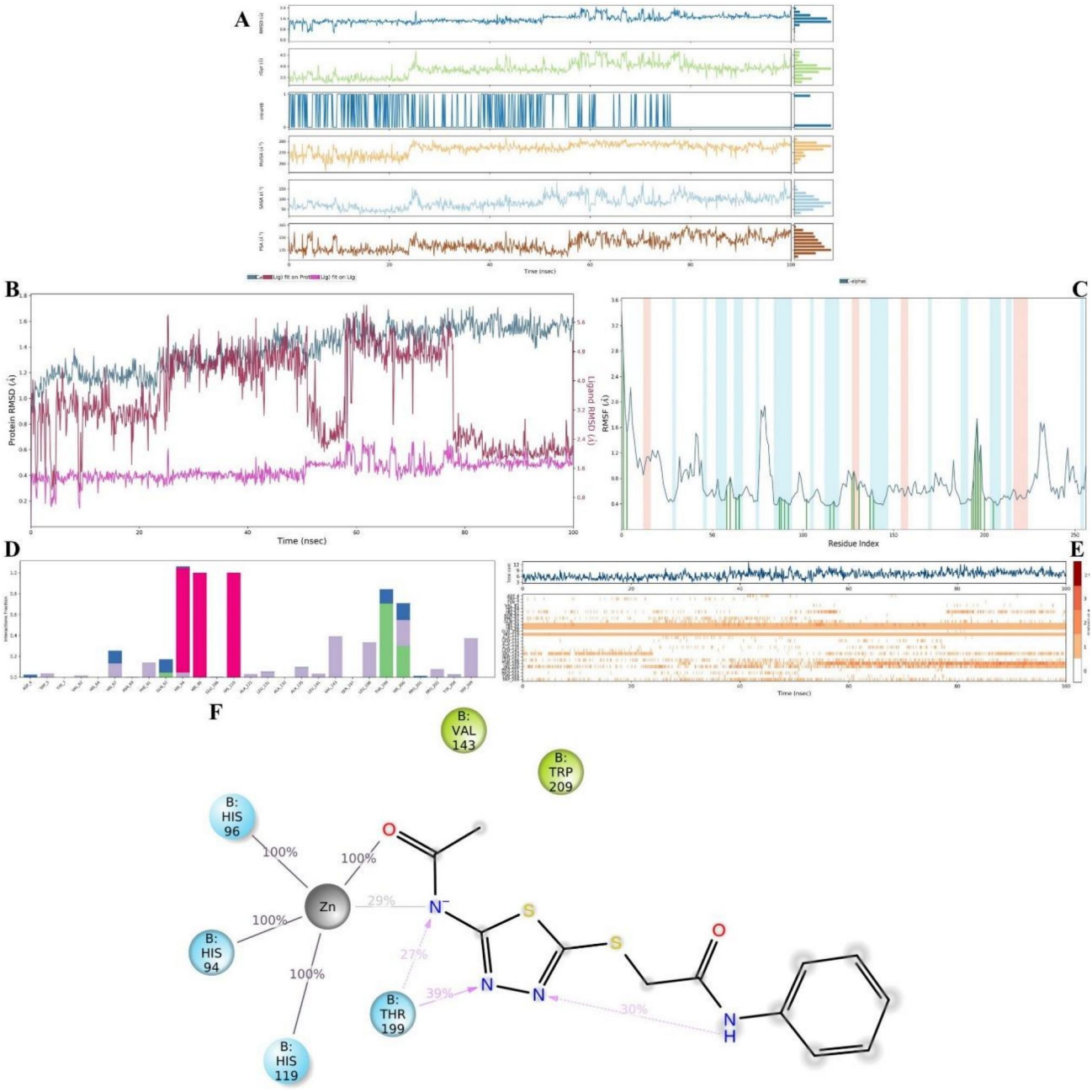

Figure 8. Plots of the MDS results for compound **5a**-*h*CA I enzyme complex. The stability properties Rg, RMSD and RMSF plots are shown in figures A, B and C, respectively; D: Interaction fraction-residue diagram; E: Total connections-residues-time plot; F: 2D interaction pose with connection strength (cut-off = 0.2) at the active region.

and enzyme surface is also crucial for the activity. Substitution on the C-2 of the thiadiazole ring with a chain of at least two carbons and a terminal aromatic ring (which also gives the advantage of interacting with Phe131) should be simultaneous with C-4 substitution with an H-bond acceptor group (such as nitro, sulphonyl amide, cyano, methoxy, etc.).

As a result, based on thiadiazole or its bioisosteres as a central nucleus, we suggest a new design idea that the compound should include an acidic group at one end with a substituent (preferably an H-bond acceptor) and a bulky aromatic ring at the other end.

The MDS results (Figure 10) indicated that the **6d**-*h*CA II complex did not show drastic changes on the Rg plot, and these values are observed between 3.2 and 4.2 Å. The RMSD diagram of the **6d**-*h*CA II complex showed that the values of ligand fit on protein, ligand fit-on-ligand, and enzyme protein properties were determined between 0 and 4.07 Å, 0 and 1.98 Å and 0 and 2.08 Å, respectively. The RMSF diagram showed that the values of α-helix and β-strands regions are under 0.8 Å. Also, the values were under 0.8 Å in the cases where loop amino acids interact with the ligand. Because of that, the findings were found to be reliable.

MDS study revealed that the pattern ligand, **6d**, interacted with metal-binding histidine residues (His94, His96 and His119), chelated to Zn^{2+} by a group of atoms including its acetamide oxygen and the thiadiazole nitrogen atoms. This

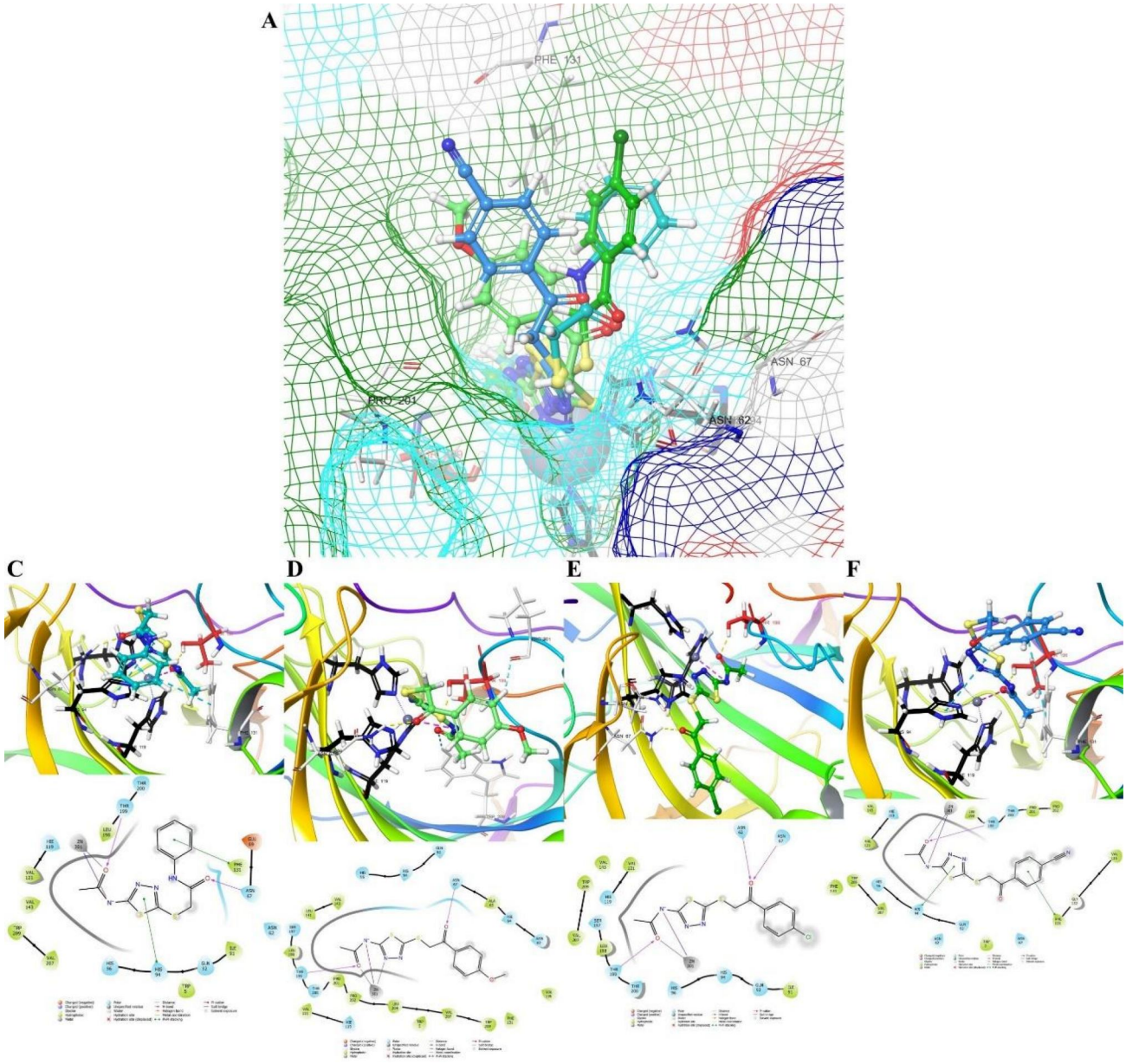

Figure 9. 2D and 3D Docking poses of compounds **5a**, **6a**, **6c** and **6d** in the active site of *h*CA II enzyme (PDBID: 3HS4). A: Superimposition of the compounds at the active pocket mapped by residue type; B: Compound **5a**; C: Compound **6a**; D: Compound **6c**; E: Compound **6d**).

chelation interaction also provided a connection with the Glu106 amino acid. Interactions with Tyr199 and Thr200 amino acids were formed *via* a water-mediated H-bond through the acetamide nitrogen. All the above interactions were formed as a result of the contribution of the small acidic acetamide group. The interaction of the acyl moiety with Asn62, Asn67 and Gln92 showed occasional occurrence.

As mentioned in the *h*CA I and *h*CA II docking sections, sequence 67 (Asn67 for *h*CA II) is an indicator of selectivity between *h*CA isoforms. Our docking results showed that the synthesized compounds have direct H-bond interactions with this sequence in both *h*CA I and *h*CA II isoforms. All compounds except **6c** displayed inhibitory activity against the enzymes. Therefore, it is thought that these compounds were optimally fitted in the binding cavities of both *h*CA I and *h*CA II enzymes. This is mainly owed to the carbon chains of the ligands, which enable them to localize into the cone-shaped active pocket. In addition, the histidine amino acid (His67 in *h*CA I) is bulkier and more lipophilic than the asparagine amino acid (Asn67 in *h*CA II), and thus, Asn67 has more affinity for the carbonyl groups that caused *h*CA II selectivity.

As a result, to gain more effective compounds against the *h*CA II enzyme, similar design strategies as presented in the MDS results of the *h*CA I enzyme are applicable. To evaluate the *h*CA II selectivity over a broad spectrum, it is necessary to test these active compounds *in vitro* against all *h*CA isoforms. However, interactions with Asn67 gave us insight that *h*CA II selectivity may be more possible.

2.5. ADME prediction

The final 1,3,4-thiadiazole compounds (**5a**–**5d, 6a**–**6d**) were *in silico* evaluated using SwissADME software (http://www.swissadme.ch/index.php) in terms of physicochemical and pharmacokinetic

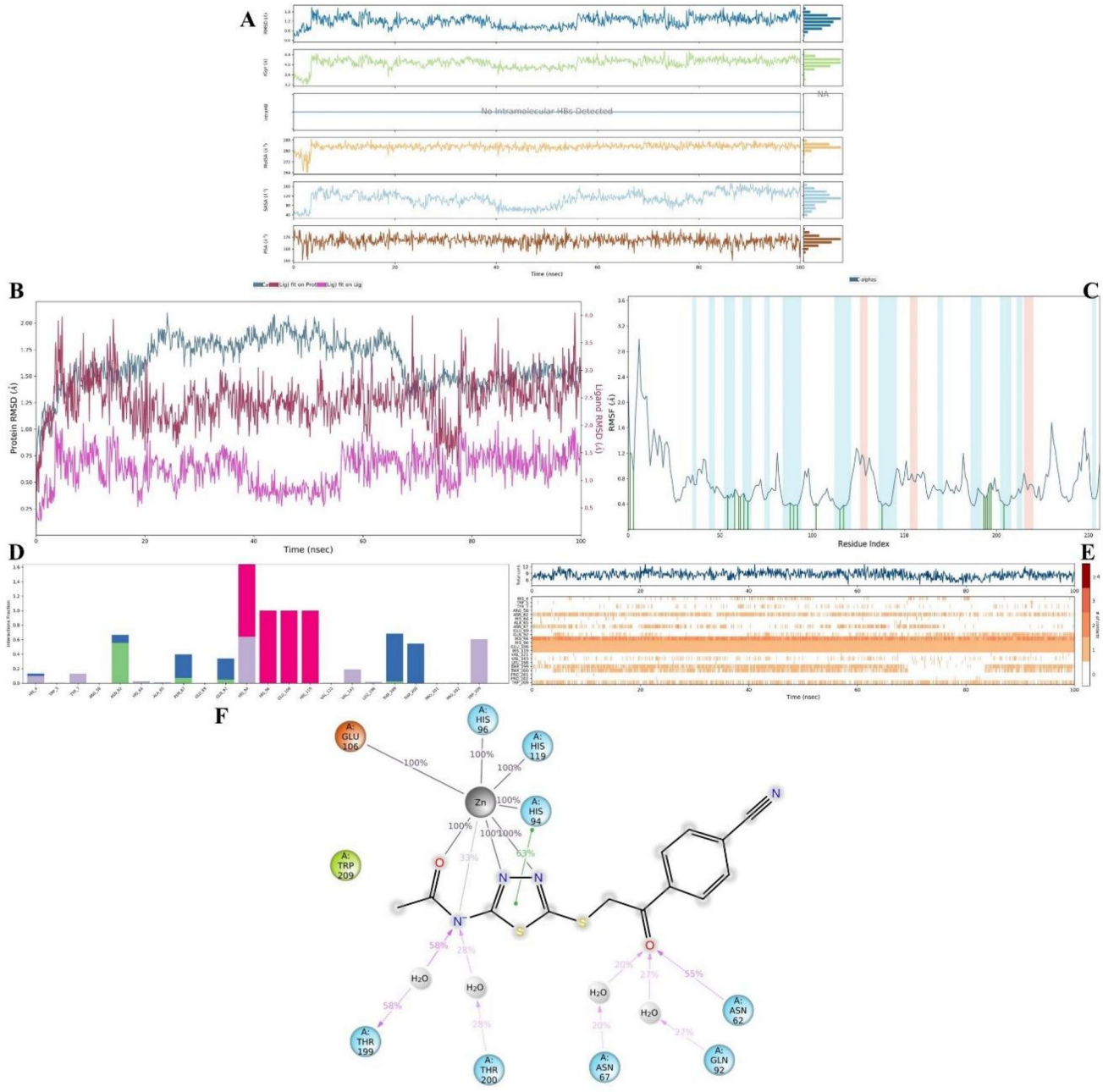

Figure 10. Plots of the MDS results for compound **6d**-*h*CA II enzyme complex. The stability properties Rg, RMSD and RMSF plots are shown in figures A–C, respectively; D: Interaction fraction-residue diagram; E: Total connections-residues-time plot; F: 2D interaction pose with connection strength (cut-off = 0.2) at the active region.

properties, and druglikeness filters as illustrated in Table 4. The evaluation showed that all of the compounds contain 4–5 hydrogen bond acceptors (HBAs). While hydrogen bond donor (HBD) is 2 in compounds **5a**–**5d** containing amide residues, it is 1 in others (**6a**–**6d**). The standard drug AAZ has an HBA of 6 and an HBD of 1. Topological polar surface area (TPSA) is in the range of 125.49–146.75 Å^2 for the synthesized compounds, 151.91 Å^2 for AAZ and 38.91 Å^2 for THA. It was observed that amide-containing derivatives have higher TPSA than other compounds. Log P, which is the measure of lipophilicity, was in the range of 1.55–2.39 for the compounds, while it was calculated as −0.70 for AAZ and 2.59 for THA. The fact that the compounds have different lipophilicity is to be expected in terms of their effectiveness in different tissues. While the water solubility (Log S) of the compounds was determined in the range of −5.05 to −4.12, indicating moderate solubility, it was observed that the water solubilities of the standard drugs were higher. The compounds were found to correlate with the lipophilicity of the Log Kp molecules, which represent skin permeability. In addition, gastrointestinal (GI) absorption of compounds **5d** and **6d** was low, while that of the rest of the compounds was estimated to be high. All of the compounds did not violate Lipinski's rules and their synthetic convenience was found to be in the range of 2.97–3.15.

3. Conclusion

The synthesized derivatives of 2-((5-acetamido-1,3,4-thiadiazole-2-yl)thio)-*N*-phenylacetamide and *N*-(5-((2-oxo-2-phenylethyl)thio)-1,3,4-thiadiazole-2-yl)acetamide showed plausible activity against both *h*CA I and *h*CA II. The most active compounds against *h*CA

Table 4. Physicochemical, pharmacokinetic and medicinal chemistry properties of the final compounds (by SwissAdme) **5a–5d** and **6a–6d**.

	Physicochemical Properties					Pharmacokinetics		Medicinal Chemistry	
Compounds	HBA	HBD	TPSA	Log $P_{o/w}$	Log S	GIA	Log K_p	RoF (V)	SA
5a	4	2	137.52	1.55	−4.12	High	−7.03	Yes (0)	3.09
5b	4	2	137.52	2.01	−4.77	High	−6.79	Yes (0)	3.05
5c	5	2	137.52	1.87	−4.22	High	−7.07	Yes (0)	3.05
5d	5	2	146.75	1.56	−4.29	Low	−7.23	Yes (0)	3.15
6a	5	1	134.72	1.89	−4.56	High	−6.78	Yes (0)	3.04
6b	4	1	125.49	1.95	−4.40	High	−6.58	Yes (0)	3.00
6c	4	1	125.49	2.39	−5.05	High	−6.43	Yes (0)	2.97
6d	5	1	149.28	1.63	−4.61	Low	−6.93	Yes (0)	3.06
AAZ	6	2	151.66	−0.70	−2.47	Low	−7.84	Yes (0)	3.00
THA	1	1	38.91	2.59	−3.18	High	−5.59	Yes (0)	2.91

HBA: H-bond acceptor; HBD: H-bond donor; TPSA: Topologic polar surface area (Å^2); Log $P_{o/w}$: Lipophilicity as *Consensus* Log $P_{o/w}$ (Average of all five predictions); Log S: Water Solubility; GIA: Gastrointestinal absorption; Log K_p: skin permeation (cm/s); RoF (V): Lipinski's Rule of Five (violation number); SA: Synthetic accessibility from 1 (very easy) to 10 (very difficult); AAZ: Acetazolamide; THA: Tacrine

I was the *N*-phenylacetamide derivatives **5a** where the *N*-phenylacetamide moiety contributed to the great activity of the compound. However, much of the activity is owed to the chelation between the acetamido substituent at C-5 of the thiadiazole ring and the zinc ion of the enzyme whether in compound **5a** or the other 2-oxo-2-phenylethyl derivatives **6a** and **6d**. Inferentially, AAZ also acts as an *h*CA I inhibitor mainly *via* the contribution of its acetamido and thiadiazole nitrogens. Thus, it is concluded that the contribution of the side chains on C-2 of the thiadiazole ring of compounds **5a**, **6a** and **6d** has a huge impact on the activity of the compounds against *h*CA I enzyme. Similar results were observed with the inhibition of *h*CA II. The variation in the activity among the designed compounds was related to the side chain on C-2 of the thiadiazole ring. Regarding the activity against AChE, only two compounds **6a** and **6c** displayed stronger inhibition than the standard THA. It was concluded by MDS and SAR investigation in this study that this activity against AChE is owed to the interaction of the compounds with Trp86, Gly120 and Tyr124 amino acids in the enzyme active site. This is because of the contribution of the 4-methoxy and 4-chlorophenyl groups in addition to the acetamido group at C-2 of thiadiazole.

4. Experimental section

4.1. Chemistry

4.1.1. General

All chemicals were purchased from Merck Chemicals (Merck KGaA, Darmstadt, Germany) and Sigma-Aldrich Chemicals (Sigma-Aldrich Corp., St. Louis, MO). The monitoring process of the reactions was achieved by thin-layer chromatography (TLC) using silica gel 60 F_{254} sheets (Merck, Darmstadt, Germany). Melting point measurements were performed using MP90 digital melting point apparatus (Mettler Toledo, OH). ^{1}H NMR and ^{13}C NMR spectral analysis was done in a Bruker 300 MHz NMR spectrophotometer (Bruker Bioscience, Billerica, MA) using DMSO-d_6 as solvent. The splitting patterns of the NMR results are abbreviated as follows: singlet: s; doublet: d; triplet: t; multiplet: m; broad singlet: brs. Also, the coupling constants (*J*) were reported as Hertz (Hz). HRMS studies were performed using an LC/MS-IT-TOF system (Shimadzu, Kyoto, Japan).

4.1.2. Synthesis of the compounds

4.1.2.1. The synthesis of 5-amino-1,3,4-thiadiazole-2-thiol (1). Anhydrous sodium carbonate (5.23 g, 49.37 mmol) and carbon disulfide (4.5 ml, 74.06 mmol) were added to a solution of thiosemicarbazide (4.5 g, 49.37 mmol) in ethanol (30 ml) at room temperature (RT). The mixture was stirred at RT for 5 min. Then, it was heated under reflux for 5 h. The completion of the reaction was monitored *via* TLC. The mixture was cooled and after removing the solvent, the residue was dissolved in ice water and acidified with 10% hydrochloric acid solution to a pH of 6. A fine light-yellow precipitate was formed which then was filtered and washed with water. Recrystallization was achieved using ethanol.

4.1.2.2. The synthesis of N-(5-mercapto-1,3,4-thiadiazole-2-yl)acetamide (2). 5-Amino-1,3,4-thiadiazole-2-thiol (2.37 g, 17.80 mmol) (1) was solved in tetrahydrofuran (THF). Triethylamine (3.6 ml, 36.6 mmol) was added, and the mixture was stirred for 5 min in an ice bath. Acetyl chloride (1.8 ml, 21.36 mmol) was then added dropwise into the mixture. After the addition of the acetyl chloride, the mixture was stirred for 2 h in the ice bath. The reaction was controlled by TLC. After completion of the reaction, the solvent was evaporated, and the solid product was washed with water and filtered. Subsequently, the crude product was recrystallized from ethanol.

4.1.2.3. General synthesis of 2-chloro-N-phenylacetamide derivatives (3a–3d). Aniline derivatives were solved in THF, and triethylamine was used as a catalyst. The final mixture was cooled in an ice bed, then 2-chloroacetyl chloride diluted in THF was cautiously added dropwise to the solution and the mixture was stirred for 2 h. TLC was used to monitor the reaction. The solvent was evaporated when the reaction was completed, and the solid product was washed with water and filtered. The crude product was then recrystallized from ethanol.

4.1.2.4. General synthesis of 2-bromoacetophenone derivatives (4a–4d). At 0 °C, 0.5 ml of hydrobromic acid was added to a solution of acetophenone derivatives (13 mmol) in acetic acid (30 ml). Bromine (13 mmol) was solved in acetic acid (15 ml) and dropped into this mixture very slowly while in an ice bath. At 0–5 °C, the mixture was stirred for 2–8 h. TLC was used to monitor the reaction. When the reaction was finished, the mixture was poured into iced water, and the product was precipitated. The final product was obtained by filtration, then washed, and dried.

4.1.2.5. General synthesis of 2-((5-acetamido-1,3,4-thiadiazole-2-yl)thio)-N-phenylacetamide derivatives (5a–5d) and N-(5-((2-oxo-2-phenylethyl)thio)-1,3,4-thiadiazole-2-yl)acetamide derivatives (6a–6d)

2-Chloro-*N*-phenylacetamide derivatives (**3a–3d**) and 2-bromoacetophenone derivatives (**4a**–**4d**) (1.43 mmol) were added to a solution of *N*-(5-mercapto-1,3,4-thiadiazole-2-yl)acetamide (**2**) (0.25 g, 1.43 mmol) in acetone (25 ml). K_2CO_3 (0.24 g, 1.72 mmol) was used as the catalyst and the mixture was stirred for 24 h at

RT. The reaction was monitored with TLC. After the reaction was completed, acetone was removed, and the crude product was washed with water and recrystallized from ethanol.

4.1.2.5.1. 2-((5-Acetamido-1,3,4-thiadiazole-2-yl)thio)-N-phenylacetamide (5a). m. p. 214–215 °C, yield 71%, ^{1}H NMR (300 MHz) (DMSO-d_6) δ (ppm): 2.17 (s, 3H, acetamide-$\underline{CH_3}$), 4.17 (s, 2H, S-$\underline{CH_2}$), 7.07 (t, J = 7.45 Hz, 1H, Ar-H), 7.31 (t, J = 8.19 Hz, 2H, Ar-H), 7.55 (d, J = 7.82 Hz, 2H, Ar-H), 10.22 (brs, 1H, -NH). ^{13}C NMR (75 MHz) (DMSO-d_6) δ (ppm): 22.77 (acetamide-$\underline{CH_3}$), 38.44 (S-$\underline{CH_2}$), 119.56, 124.06, 129.33, 139.19, 158.46, 159.43, 165.94 and 169.23. HRMS (ESI) (m/z) $[M+1]^+$ for $C_{12}H_{12}N_4O_2S_2$: calculated 309.0474; found 309.0488.

4.1.2.5.2. 2-((5-Acetamido-1,3,4-thiadiazole-2-yl)thio)-N-(4-chlorophenyl)acetamide (5b). m. p. 203–204 °C, yield 77%, ^{1}H NMR (300 MHz) (DMSO-d_6) δ (ppm): 2.17 (s, 3H, acetamide-$\underline{CH_3}$), 4.21 (s, 2H, S-$\underline{CH_2}$), 7.38 (d, J = 8.87 Hz, 2H, Ar-H), 7.60 (d, J = 8.96 Hz, 2H, Ar-H), 10.50 (brs, 1H, -NH), 12.63 (brs, 1H, -NH). ^{13}C NMR (75 MHz) (DMSO-d_6) δ (ppm): 22.76 (acetamide-$\underline{CH_3}$), 38.36 (S-$\underline{CH_2}$), 121.11, 127.59, 129.25, 138.14, 158.35, 159.42, 166.14, 169.22. HRMS (ESI) (m/z) $[M+1]^+$ for $C_{12}H_{11}ClN_4O_2S_2$: calculated 343.0085; found 343.0085.

4.1.2.5.3. 2-((5-Acetamido-1,3,4-thiadiazole-2-yl)thio)-N-(4-fluorophenyl)acetamide (5c). m. p. 188–189 °C, yield 86%, ^{1}H NMR (300 MHz) (DMSO-d_6) δ (ppm): 2.17 (s, 3H, acetamide-$\underline{CH_3}$), 4.19 (s, 2H, S-$\underline{CH_2}$), 7.16 (t, J = 8.93 Hz, 2H, Ar-H), 7.56 (d, J = 5.00 Hz, 1H, Ar-H), 7.60 (d, J = 5.00 Hz, 1H, Ar-H), 10.41 (brs, 1H, -NH), 12.61 (brs, 1H, -NH). ^{13}C NMR (75 MHz) (DMSO-d_6) δ (ppm): 22.76 (acetamide-$\underline{CH_3}$), 38.32 (S-$\underline{CH_2}$), 115.77, 116.06, 121.31, 135.60, 156.99, 158.40, 159.42, 160.18, 165.89, 169.22. HRMS (ESI) (m/z) $[M+1]^+$ for $C_{12}H_{11}FN_4O_2S_2$: calculated 327.0380; found 327.0403.

4.1.2.5.4. 2-((5-Acetamido-1,3,4-thiadiazole-2-yl)thio)-N-(4-methoxyphenyl)acetamide (5d). m. p. 220–221 °C, yield 80%, ^{1}H NMR (300 MHz) (DMSO-d_6) δ (ppm): 2.17 (s, 3H, acetamide-$\underline{CH_3}$), 3.71 (s, 3H, Ar-O$\underline{CH_3}$), 4.16 (s, 2H, S-$\underline{CH_2}$), 6.89 (d, J = 9.18 Hz, 2H, Ar-H), 7.47 (d, J = 9.04 Hz, 2H, Ar-H), 10.21 (brs, 1H, -NH), 12.61 (brs, 1H, -NH). ^{13}C NMR (75 MHz) (DMSO-d_6) δ (ppm): 22.73 (acetamide-$\underline{CH_3}$), 38.36 (S-$\underline{CH_2}$), 55.57 (Ar-O$\underline{CH_3}$), 114.39, 121.13, 132.31, 155.86, 158.53, 159.41, 165.39 and 169.21. HRMS (ESI) (m/z) $[M+1]^+$ for $C_{13}H_{14}N_4O_3S_2$: calculated 339.0580; found 339.0557.

4.1.2.5.5. N-(5-((2-(4-methoxyphenyl)-2-oxoethyl)thio)-1,3,4-thiadiazole-2-yl)acetamide (6a). m. p. 133–134 °C, yield 82%, ^{1}H NMR (300 MHz) (DMSO-d_6) δ (ppm): 2.16 (s, 3H, acetamide-$\underline{CH_3}$), 3.85 (s, 3H, Ar-O$\underline{CH_3}$), 4.98 (s, 2H, S-$\underline{CH_2}$), 7.07 (d, J = 8.94 Hz, 2H, Ar-H), 8.01 (d, J = 8.92 Hz, 2H, Ar-H), 12.59 (brs, 1H, -NH). ^{13}C NMR (75 MHz) (DMSO-d_6) δ (ppm): 22.71 (acetamide-$\underline{CH_3}$), 41.59 (S-$\underline{CH_2}$), 56.13 (Ar-O$\underline{CH_3}$), 114.51, 128.43, 131.39, 158.43, 159.25, 164.07, 169.19 and 191.85. HRMS (ESI) (m/z) $[M+1]^+$ for $C_{13}H_{13}N_3O_3S_2$: calculated 324.0471; found 324.0452.

4.1.2.5.6. N-(5-((2-oxo-2-phenylethyl)thio)-1,3,4-thiadiazole-2-yl)acetamide (6b). m. p. 197–198 °C, yield 79%, ^{1}H NMR (300 MHz) (DMSO-d_6) δ (ppm): 2.17 (s, 3H, acetamide-$\underline{CH_3}$), 5.03 (s, 2H, S-$\underline{CH_2}$), 7.56 (t, J = 7.32 Hz, 2H, Ar-H), 7.69 (t, J = 7.40 Hz, 1H, Ar-H), 8.04 (d, J = 7.10 Hz, 2H, Ar-H), 12.58 (brs, 1H, -NH). ^{13}C NMR (75 MHz) (DMSO-d_6) δ (ppm): 22.72 (acetamide-$\underline{CH_3}$), 41.78 (S-$\underline{CH_2}$), 128.96, 129.32, 134.31, 135.60, 158.23, 159.29, 169.20 and 193.54. HRMS (ESI) (m/z) $[M+1]^+$ for $C_{12}H_{11}N_3O_2S_2$: calculated 294.0365; found 294.0368.

4.1.2.5.7. N-(5-((2-(4-chlorophenyl)-2-oxoethyl)thio)-1,3,4-thiadiazole-2-yl)acetamide (6c). m. p. 179–180 °C, yield 88%, ^{1}H NMR (300 MHz) (DMSO-d_6) δ (ppm): 2.17 (s, 3H, acetamide-$\underline{CH_3}$), 5.02 (s, 2H, S-$\underline{CH_2}$), 7.63 (d, J = 8.61 Hz, 2H, Ar-H), 8.05 (d, J = 8.63 Hz, 2H, Ar-H), 12.59 (brs, 1H, -NH). ^{13}C NMR (75 MHz) (DMSO-d_6) δ (ppm): 22.71 (acetamide-$\underline{CH_3}$), 41.68 (S-$\underline{CH_2}$), 129.43, 130.88, 134.31, 139.22, 158.04, 159.35, 169.20 and 192.69. HRMS (ESI) (m/z) $[M+1]^+$ for $C_{12}H_{10}ClN_3O_2S_2$: calculated 327.9976; found 327.9978.

4.1.2.5.8. N-(5-((2-(4-cyanophenyl)-2-oxoethyl)thio)-1,3,4-thiadiazole-2-yl)acetamide (6d). m. p. 184–185 °C, yield 89%, ^{1}H NMR (300 MHz) (DMSO-d_6) δ (ppm): 2.51 (s, 3H, acetamide-$\underline{CH_3}$), 5.05 (s, 2H, S-$\underline{CH_2}$), 8.06 (d, J = 8.30 Hz, 2H, Ar-H), 8.19 (d, J = 7.61 Hz, 2H, Ar-H), 12.59 (brs, 1H, -NH). ^{13}C NMR (75 MHz) (DMSO-d_6) δ (ppm): 22.25 (acetamide-$\underline{CH_3}$), 40.28 (S-$\underline{CH_2}$), 114.60, 117.07, 128.08, 131.85, 137.43, 156.32, 157.98, 167.76 and 191.72. HRMS (ESI) (m/z) $[M+1]^+$ for $C_{13}H_{10}N_4O_2S_2$: calculated 319.0318; found 319.0322.

4.2. Biochemistry

4.2.1. hCA and AChE inhibitory activity study

Verpoorte's approach of examining the change in absorbance at 348 nm (Verpoorte et al., 1967) was used to assess the esterase activity of the *h*CAs, *h*CA I and II isoforms to determine the inhibitory effects of novel 1,3,4-thiadiazole derivatives. Standard drugs, AAZ (PubChem CID: 1986) and THA (PubChem CID: 1935) were used as inhibitors of *h*CAs and AChE, respectively. The synthesized compounds and standards were dissolved in DMSO at a starting concentration of 1 mg/ml. The final reaction mixture contained DMSO at a concentration of around 1%. As in our earlier experiments (Güleç et al., 2022; Lolak et al., 2022; Osmaniye, Türkeş, et al., 2022), the *h*CA isoforms' activity was assessed using the same substrate, 4-nitrophenyl acetate (PubChem CID: 13243). Additionally, using acetylthiocholine iodide (PubChem CID: 74629) as the substrate at 412 nm, Ellman's technique (Ellman et al., 1961) was used to assess the *in vitro* effects of these 1,3,4-thiadiazole derivatives on AChE (Askin et al., 2021). An enzyme unit is an enzyme required to catalyze the reaction of 1 mol of substrate per minute at 25 °C. Kinetic tests with varying substrate and molecule concentrations were carried out to examine these derivatives' *in vitro* inhibition mechanisms. Three measurements were performed on each sample. Michaelis–Menten curves, Lineweaver–Burk plots, K_I constants, R^2 coefficients and types of inhibition

were all produced using the observed data as previously reported by Türkeş et al. (2021, 2022).

4.2.2. Statistical study

GraphPad Prism version 9 for Mac (GraphPad Software, La Jolla, CA) was used for data analysis and graph creation. SigmaPlot version 12 for Windows (Systat Software, San Jose, CA) was used to calculate the inhibition constants. The fit of enzyme inhibition models was examined using the additional sum-of-squares F test and the AICc method. The data were presented as mean ± standard error of the mean (95% confidence intervals). When the p value was less than 0.05, differences between data sets were deemed statistically significant.

4.3. In silico methods

4.3.1. Pharmacokinetic calculations

The SwissADME online tool was used to conduct *in silico* calculations of certain physicochemical properties required to predict the pharmacokinetic properties of compounds **5a–5d** and **6a–6d** (Jatczak et al., 2014). Table 4 displays the values of HBAs, HBDs, TPSA, lipophilicity (Log P), water solubility (Log S), skin permeation (Log K_p), absorption from the gastrointestinal absorption (GIA) and other variables. All of the synthesized compounds were predicted to have high membrane permeability (BBB/GI). This is affected mainly by optimum lipophilicity with values $\leq$5 (log P 1.63–2.39) as required by Lipinski's Rule of Five, and also an acceptable range of polarity (Khan et al., 2016). The drug-like properties of the compounds were evaluated and the results showed the values to be in the required range of Lipinski's rule.

4.3.2. Molecular docking, molecular dynamic simulations and SAR studies

In silico approaches are used for several reasons by pharmaceutical chemists (Asseri et al., 2022; Bassani et al., 2022; Ekins et al., 2007; Rocca et al., 2022) and one of them is to demonstrate the structure–activity relationship by observing the interactions of active compounds with proteins, environmental variables and the stability of the ligand-protein complex over time as in this study. This relationship provides foresight for the evaluation of the potent compound(s) found in the clinical stages. In addition, it provides a basis for the creation of design strategies to be used in the discovery of new compounds that might be more effective, less costly and have fewer side effects.

According to *in vitro* results, the docking procedures were applied to *h*CA I, *h*CA II and AChE enzymes. The crystal structures of those proteins were retrieved from the protein data bank server (www.rcsb.org; PDBID: 2NMX, 3HS4, 4EY7, respectively). As in previous studies (Dawbaa et al., 2022; Evren, Demokrat, et al., 2022; Evren, Karaduman, et al., 2022; Güzel et al., 2023), The Protein Preparation Wizard protocol of the Schrödinger Suite 2020 was then used to build the structure of the enzymes. The protonation states as well as the atom types were assigned using the LigPrep module Schrödinger Release (2020c) in order to prepare the ligands. Besides that, bond orders and hydrogen atoms were added to the structures. The Glide module (2020b) was used for grid generation. Docking runs were all optimized by using the standard precision (SP) docking mode.

The MDSs were performed using Schrödinger's Maestro Desmond interface program 2020-3 release (2020a). Each MDS study was achieved for a period of 100 ns. MDS studies were carried out to verify the *in vitro* results by evaluating the stability of the identified hits in their active sites. The procedure of MDS in this study was carried out according to the method detailed in previous studies (Acar Çevik et al., 2022; Evren, Nuha, et al., 2022; Pagnozzi et al., 2022; Taraphder et al., 2016). All systems were set up using 'System Builder' in Maestro. The complex structure was subjected to energy minimization (OPLS3e standard force field). The hydration was achieved using the transferable intermolecular potential with the three-point water model. Na^+ and Cl^- ions were selected as system-neutralizing ions. Next, MDS was performed upon finishing the setup of the system. The MDS calculations gave illustrative data regarding the Rg, RMSF and RMSD.

4.3.3. DFT studies

Theoretical analyses for our active compounds were carried out using the Gaussian 09 W package (Gaussian09, 2009) and GaussView version 5.0 (Dennington et al., 2009) molecular visualization tools. The three-dimensional configuration of the test compounds was optimized using density functional theory (DFT), Becke's three-parameter hybrid functional (B3LYP) approach (Becke, 1992) and the 6-31 G (d, p) basis set in the ground state and gas phase. HOMO and LUMO energy values of the compounds were calculated at a time-dependent (TD)-DFT level to describe intramolecular charge-transfer interactions.

Chemical reactivity parameters like ionization potential I ($I = -E_{HOMO}$), electron affinity A ($A = -E_{LUMO}$), electronegativity χ ($\chi = (I + A)/2$), chemical hardness η ($\eta = (I\text{-}A)/2$), chemical softness S ($S = 1/2\eta$), chemical potential μ ($\mu = -(I + A)/2$) and electrophilicity index ω ($\omega = \mu^2/2\eta$) of the molecular groups were calculated using HOMO–LUMO energy values.

The total electric dipole moment (μ_{tot}) is calculated theoretically by using the following equation:

$$\mu_{tot} = \left(\mu_x{}^2 + \mu_y{}^2 + \mu_z{}^2\right)^{1/2} \quad (1)$$

Acknowledgments

We would like to thank MERLAB and BİBAM, Anadolu University for spectral analysis.

Author contributions

Drug design: S.D. and A.E.E., chemical synthesis: S.D., chemical analysis: S.D. and D.N., *in vitro* enzyme tests: C.T., Y.D. and Ş.B., molecular docking & Molecular dynamic simulations: A.E.E, DFT calculations: D.N., analysis and evaluation of the results: L.Y. and Ş.B., article's writer: L.Y., Ş.B., A.E.E., D.N., S.D., C.T. and Y.D., article review: L.Y., S.D., A.E.E. and D.N.

Disclosure statement

The author confirms that this article content has no conflict of interest.

Funding

The author(s) reported there is no funding associated with the work featured in this article.

ORCID

Sam Dawbaa http://orcid.org/0000-0001-7001-0739
Cüneyt Türkeş http://orcid.org/0000-0002-2932-2789
Demokrat Nuha http://orcid.org/0000-0002-7271-6791
Yeliz Demir http://orcid.org/0000-0001-8320-8517
Asaf Evrim Evren http://orcid.org/0000-0002-8651-826X
Leyla Yurttaş http://orcid.org/0000-0002-0957-6044
Şükrü Beydemir http://orcid.org/0000-0003-3667-6902

References

Abas, M., Bahadur, A., Ashraf, Z., Iqbal, S., Rajoka, M. S. R., Rashid, S. G., Jabeen, E., Iqbal, Z., Abbas, Q., Bais, A., Hassan, M., Liu, G., Feng, K., Lee, S. H., Nawaz, M., & Qayyum, M. A. (2021). Designing novel anticancer sulfonamide based 2, 5-disubstituted-1, 3, 4-thiadiazole derivatives as potential carbonic anhydrase inhibitor. *Journal of Molecular Structure*, *1246*, 131145. https://doi.org/10.1016/j.molstruc.2021.131145

Abdel-Hamid, M. K., Abdel-Hafez, A. A., El-Koussi, N. A., Mahfouz, N. M., Innocenti, A., & Supuran, C. T. (2007). Design, synthesis, and docking studies of new 1, 3, 4-thiadiazole-2-thione derivatives with carbonic anhydrase inhibitory activity. *Bioorganic & Medicinal Chemistry*, *15*(22), 6975–6984. https://doi.org/10.1016/j.bmc.2007.07.044

Acar Çevik, U., Işık, A., Evren, A., Kapusız, Ö., Gül, Ü., Özkay, Y., & Kaplancıklı, Z. (2022). Synthesis of new benzimidazole derivatives containing 1, 3, 4-thiadiazole: Their in vitro antimicrobial, in silico molecular docking and molecular dynamic simulations studies. *SAR and QSAR in Environmental Research*, *33*(11), 899–914. https://doi.org/10.1080/1062936X.2022.2149620

Alterio, V., Di Fiore, A., D'Ambrosio, K., Supuran, C. T., & De Simone, G. (2012). Multiple binding modes of inhibitors to carbonic anhydrases: How to design specific drugs targeting 15 different isoforms? *Chemical Reviews*, *112*(8), 4421–4468. https://doi.org/10.1021/cr200176r

Aouad, M. R., Almehmadi, M. A., Albelwi, F. F., Teleb, M., Tageldin, G. N., Abu-Serie, M. M., Hagar, M., & Rezki, N. (2022). Targeting the interplay between MMP-2, CA II and VEGFR-2 via new sulfonamide-tethered isomeric triazole hybrids; Microwave-assisted synthesis, computational studies and evaluation. *Bioorganic Chemistry*, *124*, 105816. https://doi.org/10.1016/j.bioorg.2022.105816

Askin, S., Tahtaci, H., Türkeş, C., Demir, Y., Ece, A., Çiftçi, G. A., & Beydemir, Ş. (2021). Design, synthesis, characterization, in vitro and in silico evaluation of novel imidazo [2, 1-b][1, 3, 4] thiadiazoles as highly potent acetylcholinesterase and non-classical carbonic anhydrase inhibitors. *Bioorganic Chemistry*, *113*, 105009. https://doi.org/10.1016/j.bioorg.2021.105009

Asseri, A. H., Alam, M. J., Alzahrani, F., Khames, A., Pathan, M. T., Abourehab, M. A. S., Hosawi, S., Ahmed, R., Sultana, S. A., Alam, N. F., Alam, N.-U., Alam, R., Samad, A., Pokhrel, S., Kim, J. K., Ahammad, F., Kim, B., & Tan, S. C. (2022). Toward the identification of natural antiviral drug candidates against merkel cell polyomavirus: Computational drug design approaches. *Pharmaceuticals*, *15*(5), 501. https://doi.org/10.3390/ph15050501

Atmaram, U. A., & Roopan, S. M. (2022). Biological activity of oxadiazole and thiadiazole derivatives. *Applied Microbiology and Biotechnology*, *106*(9–10), 3489–3505. https://doi.org/10.1007/s00253-022-11969-0

Bassani, D., Pavan, M., Bolcato, G., Sturlese, M., & Moro, S. (2022). Re-exploring the ability of common docking programs to correctly reproduce the binding modes of non-covalent inhibitors of SARS-CoV-2 protease MPRO. *Pharmaceuticals*, *15*(2), 180. https://doi.org/10.3390/ph15020180

Becke, A. D. (1992). Density-functional thermochemistry. I. The effect of the exchange-only gradient correction. *The Journal of Chemical Physics*, *96*(3), 2155–2160. https://doi.org/10.1063/1.462066

Bulos, J. A., Guo, R., Wang, Z., DeLessio, M. A., Saven, J. G., & Dmochowski, I. J. (2021). Design of a superpositively charged enzyme: Human carbonic anhydrase II variant with ferritin encapsulation and immobilization. *Biochemistry*, *60*(47), 3596–3609. https://doi.org/10.1021/acs.biochem.1c00515

Chen, A. Y., Adamek, R. N., Dick, B. L., Credille, C. V., Morrison, C. N., & Cohen, S. M. (2018). Targeting metalloenzymes for therapeutic intervention. *Chemical Reviews*, *119*(2), 1323–1455. https://doi.org/10.1021/acs.chemrev.8b00201

Coşkun, G., Birgül, K., Evren, A. E., Küçükgüzel, ŞG., & Ülgen, M. (2023). In Silico studies and in vitro microsomal metabolism of potent MetAP2 inhibitor and in vivo tumor suppressor for prostate cancer: A thioether-triazole hybrid. *Acıbadem Üniversitesi Sağlık Bilimleri Dergisi*, *14*(1), 10–23. https://doi.org/10.31067/acusaglik.1210129

Dawbaa, S., Evren, A. E., Sağlik, B. N., Gundogdu-Karaburun, N., & Karaburun, A. C. (2022). Biological activity evaluation of novel monoamine oxidase inhibitory compounds targeting Parkinson disease. *Future Medicinal Chemistry*, *14*(22), 1663–1679. https://doi.org/10.4155/fmc-2022-0167

Dennington, R., Keith, T., & Millam, J. (2009). *GaussView, version 5*. Shawnee Mission: Semichem Inc.

Di Fiore, A., De Luca, V., Langella, E., Nocentini, A., Buonanno, M., Monti, S. M., Supuran, C. T., Capasso, C., & De Simone, G. (2022). Biochemical, structural, and computational studies of a γ-carbonic anhydrase from the pathogenic bacterium Burkholderia pseudomallei. *Computational and Structural Biotechnology Journal*, *20*, 4185–4194. https://doi.org/10.1016/j.csbj.2022.07.033

Dokmanić, I., Sikić, M., & Tomić, S. (2008). Metals in proteins: Correlation between the metal-ion type, coordination number and the amino-acid residues involved in the coordination. *Acta Crystallographica Section D, Biological Crystallography*, *64*(Pt 3), 257–263. https://doi.org/10.1107/S090744490706595X

Dvir, H., Silman, I., Harel, M., Rosenberry, T. L., & Sussman, J. L. (2010). Acetylcholinesterase: From 3D structure to function. *Chemico-Biological Interactions*, *187*(1–3), 10–22. https://doi.org/10.1016/j.cbi.2010.01.042

Ekins, S., Mestres, J., & Testa, B. (2007). In silico pharmacology for drug discovery: Methods for virtual ligand screening and profiling. *British Journal of Pharmacology*, *152*(1), 9–20. https://doi.org/10.1038/sj.bjp.0707305

Ellman, G. L., Courtney, K. D., Andres, V., & Feather-Stone, R. M. (1961). A new and rapid colorimetric determination of acetylcholinesterase activity. *Biochemical Pharmacology*, *7*(2), 88–95. https://doi.org/10.1016/0006-2952(61)90145-9

Ergena, A., Rajeshwar, Y., & Solomon, G. (2022). Synthesis and diuretic activity of substituted 1, 3, 4-thiadiazoles. *Scientifica*, *2022*, 3011531–3011539. https://doi.org/10.1155/2022/3011531

Evren, A. E., Demokrat, N., & Yurttaş, L. (2022). Focusing on the moderately active compound (MAC) in the design and development of strategies to optimize the apoptotic effect by molecular mechanics techniques. *European Journal of Life Sciences*, *1*(3), 118–126. https://doi.org/10.55971/EJLS.1209591

Evren, A. E., Karaduman, A. B., Sağlik, B. N., Özkay, Y., & Yurttaş, L. (2022). Investigation of novel quinoline–thiazole derivatives as antimicrobial agents: In Vitro and in silico approaches. *ACS Omega*, *8*(1), 1410–1429. https://doi.org/10.1021/acsomega.2c06871

Evren, A. E., Nuha, D., Dawbaa, S., Sağlık, B. N., & Yurttaş, L. (2022). Synthesis of novel thiazolyl hydrazone derivatives as potent dual monoamine oxidase-aromatase inhibitors. *European Journal of Medicinal Chemistry*, *229*, 114097. https://doi.org/10.1016/j.ejmech.2021.114097

Fu, X., Li, S., Jing, F., Wang, X., Li, B., Zhao, J., Liu, Y., & Chen, B. (2016). Synthesis and biological evaluation of novel 1, 3, 4-thiadiazole derivatives incorporating benzisoselenazolone scaffold as potential

antitumor agents. *Medicinal Chemistry*, *12*(7), 631–639. https://doi.org/10.2174/1573406412666160201120806

Fukui, K. (1982). Role of frontier orbitals in chemical reactions. *Science*, *218*(4574), 747–754. https://doi.org/10.1126/science.218.4574.747

Gaussian09, R. A. (2009). *1, mj frisch, gw trucks, hb schlegel, ge scuseria, ma robb, jr cheeseman, g. Scalmani, v. Barone, b. Mennucci, ga petersson et al* (Vol. 121, pp. 150–166). Gaussian. Inc.

Gowda, K., Swarup, H. A., Nagarakere, S. C., Rangappa, S., Kanchugarkoppal, R. S., & Kempegowda, M. (2020). Structural studies of 2, 5-disubstituted 1, 3, 4-thiadiazole derivatives from dithioesters under the mild condition: Studies on antioxidant, antimicrobial activities, and molecular docking. *Synthetic Communications*, *50*(10), 1528–1544. https://doi.org/10.1080/00397911.2020.1745843

Gregory, D. S., Martin, A. C., Cheetham, J. C., & Rees, A. R. (1993). The prediction and characterization of metal binding sites in proteins. *Protein Engineering*, *6*(1), 29–35. https://doi.org/10.1093/protein/6.1.29

Güleç, Ö., Türkeş, C., Arslan, M., Demir, Y., Yeni, Y., Hacımüftüoğlu, A., Ereminsoy, E., Küfrevioğlu, Ö. İ., & Beydemir, Ş. Ş (2022). Cytotoxic effect, enzyme inhibition, and in silico studies of some novel N-substituted sulfonyl amides incorporating 1, 3, 4-oxadiazol structural motif. *Molecular Diversity*, *26*(5), 2825–2845. https://doi.org/10.1007/s11030-022-10422-8

Güzel-Akdemir, Ö., Akdemir, A., Karalı, N., & Supuran, C. T. (2015). Discovery of novel isatin-based sulfonamides with potent and selective inhibition of the tumor-associated carbonic anhydrase isoforms IX and XII. *Organic & Biomolecular Chemistry*, *13*(23), 6493–6499. https://doi.org/10.1039/c5ob00688k

Güzel, E., Acar Çevik, U., Evren, A. E., Bostancı, H. E., Gül, Ü. D., Kayış, U., Özkay, Y., & Kaplancıklı, Z. A. (2023). Synthesis of benzimidazole-1, 2, 4-triazole derivatives as potential antifungal agents targeting 14α-demethylase. *ACS Omega*, *8*(4), 4369–4384. https://doi.org/10.1021/acsomega.2c07755

Jatczak, M., Muylaert, K., De Coen, L. M., Keemink, J., Wuyts, B., Augustijns, P., & Stevens, C. V. (2014). Straightforward entry to pyrido [2, 3-d] pyrimidine-2, 4 (1H, 3H)-diones and their ADME properties. *Bioorganic & Medicinal Chemistry*, *22*(15), 3947–3956. https://doi.org/10.1016/j.bmc.2014.06.009

Kakakhan, C., Türkeş, C., Güleç, Ö., Demir, Y., Arslan, M., Özkemahlı, G., & Beydemir, Ş. Ş (2023). Exploration of 1, 2, 3-triazole linked benzenesulfonamide derivatives as isoform selective inhibitors of human carbonic anhydrase. *Bioorganic & Medicinal Chemistry*, *77*, 117111. https://doi.org/10.1016/j.bmc.2022.117111

Kalinin, S., Kovalenko, A., Valtari, A., Nocentini, A., Gureev, M., Urtti, A., Korsakov, M., Supuran, C. T., & Krasavin, M. (2022). 5-(Sulfamoyl) thien-2-yl 1, 3-oxazole inhibitors of carbonic anhydrase II with hydrophilic periphery. *Journal of Enzyme Inhibition and Medicinal Chemistry*, *37*(1), 1005–1011. https://doi.org/10.1080/14756366.2022.2056733

Karaburun, A. Ç., Acar Çevik, U., Osmaniye, D., Sağlık, B. N., Kaya Çavuşoğlu, B., Levent, S., Özkay, Y., Koparal, A. S., Behçet, M., & Kaplancıklı, Z. A. (2018). Synthesis and evaluation of new 1, 3, 4-thiadiazole derivatives as potent antifungal agents. *Molecules (Basel, Switzerland)*, *23*(12), 3129. https://doi.org/10.3390/molecules23123129

Kasımoğulları, R., Bülbül, M., Arslan, B. S., & Gökçe, B. (2010). Synthesis, characterization and antiglaucoma activity of some novel pyrazole derivatives of 5-amino-1, 3, 4-thiadiazole-2-sulfonamide. *European Journal of Medicinal Chemistry*, *45*(11), 4769–4773. https://doi.org/10.1016/j.ejmech.2010.07.041

Khan, F. A. K., Patil, R. H., Shinde, D. B., & Sangshetti, J. N. (2016). Bacterial Peptide deformylase inhibition of cyano substituted biaryl analogs: Synthesis, in vitro biological evaluation, molecular docking study and in silico ADME prediction. *Bioorganic & Medicinal Chemistry*, *24*(16), 3456–3463. https://doi.org/10.1016/j.bmc.2016.05.051

Lolak, N., Akocak, S., Durgun, M., Duran, H. E., Necip, A., Türkeş, C., Işık, M., & Beydemir, Ş. (2022). Novel bis-ureido-substituted sulfaguanidines and sulfisoxazoles as carbonic anhydrase and acetylcholinesterase inhibitors. *Molecular Diversity*, *27*(4), 1735–1749. https://doi.org/10.1007/s11030-022-10527-0

Long, D. D., Frieman, B., Hegde, S. S., Hill, C. M., Jiang, L., Kintz, S., Marquess, D. G., Purkey, H., Shaw, J.-P., Steinfeld, T., Wilson, M. S., & Wrench, K. (2013). A multivalent approach towards linked dual-pharmacology prostaglandin F receptor agonist/carbonic anhydrase-II inhibitors for the treatment of glaucoma. *Bioorganic & Medicinal Chemistry Letters*, *23*(4), 939–943. https://doi.org/10.1016/j.bmcl.2012.12.058

Lotfi, S., Rahmani, T., Hatami, M., Pouramiri, B., Kermani, E. T., Rezvannejad, E., Mortazavi, M., Fathi Hafshejani, S., Askari, N., Pourjamali, N., & Zahedifar, M. (2020). Design, synthesis and biological assessment of acridine derivatives containing 1, 3, 4-thiadiazole moiety as novel selective acetylcholinesterase inhibitors. *Bioorganic Chemistry*, *105*, 104457. https://doi.org/10.1016/j.bioorg.2020.104457

Luque, F., Orozco, M., Bhadane, P., & Gadre, S. (1993). SCRF calculation of the effect of water on the topology of the molecular electrostatic potential. *The Journal of Physical Chemistry*, *97*(37), 9380–9384. https://doi.org/10.1021/j100139a021

Nocentini, A., Supuran, C. T., & Capasso, C. (2021). An overview on the recently discovered iota-carbonic anhydrases. *Journal of Enzyme Inhibition and Medicinal Chemistry*, *36*(1), 1988–1995. https://doi.org/10.1080/14756366.2021.1972995

Osmaniye, D., Evren, A. E., Sağlık, B. N., Levent, S., Özkay, Y., & Kaplancıklı, Z. A. (2022). Design, synthesis, biological activity, molecular docking, and molecular dynamics of novel benzimidazole derivatives as potential AChE/MAO-B dual inhibitors. *Archiv Der Pharmazie*, *355*(3), e2100450. https://doi.org/10.1002/ardp.202100450

Osmaniye, D., Türkeş, C., Demir, Y., Özkay, Y., Beydemir, Ş., & Kaplancıklı, Z. A. (2022). Design, synthesis, and biological activity of novel dithiocarbamate-methylsulfonyl hybrids as carbonic anhydrase inhibitors. *Archiv Der Pharmazie*, *355*(8), e2200132. https://doi.org/10.1002/ardp.202200132

Pagnozzi, D., Pala, N., Biosa, G., Dallocchio, R., Dessì, A., Singh, P. K., Rogolino, D., Di Fiore, A., De Simone, G., Supuran, C. T., & Sechi, M. (2022). Interaction studies between carbonic anhydrase and a sulfonamide inhibitor by experimental and theoretical approaches. *ACS Medicinal Chemistry Letters*, *13*(2), 271–277. https://doi.org/10.1021/acsmedchemlett.1c00644

Politzer, P., & Murray, J. S. (2002). The fundamental nature and role of the electrostatic potential in atoms and molecules. *Theoretical Chemistry Accounts*, *108*(3), 134–142. https://doi.org/10.1007/s00214-002-0363-9

Rocca, R., Scionti, F., Nadai, M., Moraca, F., Maruca, A., Costa, G., Catalano, R., Juli, G., Di Martino, M. T., Ortuso, F., Alcaro, S., Tagliaferri, P., Tassone, P., Richter, S. N., & Artese, A. (2022). Chromene derivatives as selective TERRA G-quadruplex RNA binders with antiproliferative properties. *Pharmaceuticals*, *15*(5), 548. https://doi.org/10.3390/ph15050548

Schrödinger Release. (2020a). *Schrödinger release 2020–3, desmond*. Schrödinger, LLC.

Schrödinger Release. (2020b). *Schrödinger Release 2020–3, glide*. Schrödinger, LLC.

Schrödinger Release. (2020c). *Schrödinger release. 2020–3: LigPrep 2020*. Schrödinger, LLC.

Skrzypek, A., Matysiak, J., Karpińska, M., Czarnecka, K., Krȩcisz, P., Stary, D., Kukułowicz, J., Paw, B., Bajda, M., Szymański, P., & Niewiadomy, A. (2021). Biological evaluation and molecular docking of novel 1, 3, 4-thiadiazole-resorcinol conjugates as multifunctional cholinesterases inhibitors. *Bioorganic Chemistry*, *107*, 104617. https://doi.org/10.1016/j.bioorg.2020.104617

Supuran, C. T., & Clare, B. W. (1999). Carbonic anhydrase inhibitors–Part 57: Quantum chemical QSAR of a group of 1, 3, 4-thiadiazole-and 1, 3, 4-thiadiazoline disulfonamides with carbonic anhydrase inhibitory properties. *European Journal of Medicinal Chemistry*, *34*(1), 41–50. https://doi.org/10.1016/S0223-5234(99)80039-7

Supuran, C. T., & Scozzafava, A. (2000a). Carbonic anhydrase inhibitors-Part 94. 1, 3, 4-Thiadiazole-2-sulfonamide derivatives as antitumor agents? *European Journal of Medicinal Chemistry*, *35*(9), 867–874. https://doi.org/10.1016/s0223-5234(00)00169-0

Supuran, C. T., & Scozzafava, A. (2000b). Carbonic anhydrase inhibitors and their therapeutic potential. *Expert Opinion on Therapeutic Patents*, *10*(5), 575–600. https://doi.org/10.1517/13543776.10.5.575

Taraphder, S., Maupin, C. M., Swanson, J. M., & Voth, G. A. (2016). Coupling protein dynamics with proton transport in human carbonic anhydrase II. *The Journal of Physical Chemistry. B*, *120*(33), 8389–8404. https://doi.org/10.1021/acs.jpcb.6b02166

Thiry, A., Supuran, C. T., Masereel, B., & Dogné, J. M. (2008). Recent developments of carbonic anhydrase inhibitors as potential anticancer drugs. *Journal of Medicinal Chemistry*, *51*(11), 3051–3056. https://doi.org/10.1021/jm701526d

Turan Yücel, N., Evren, A. E., Kandemir, Ü., & Can, Ö. D. (2022). Antidepressant-like effect of tofisopam in mice: A behavioural, molecular docking and MD simulation study. *Journal of Psychopharmacology (Oxford, England)*, *36*(7), 819–835. https://doi.org/10.1177/02698811221095528

Türkeş, C., Akocak, S., Işık, M., Lolak, N., Taslimi, P., Durgun, M., Gülçin, İ., Budak, Y., & Beydemir, Ş. (2022). Novel inhibitors with sulfamethazine backbone: Synthesis and biological study of multi-target cholinesterases and α-glucosidase inhibitors. *Journal of Biomolecular Structure & Dynamics*, *40*(19), 8752–8764. https://doi.org/10.1080/07391102.2021.1916599

Türkeş, C., Demir, Y., & Beydemir, Ş. Ş (2021). Calcium channel blockers: Molecular docking and inhibition studies on carbonic anhydrase I and II isoenzymes. *Journal of Biomolecular Structure & Dynamics*, *39*(5), 1672–1680. https://doi.org/10.1080/07391102.2020.1736631

Verpoorte, J. A., Mehta, S., & Edsall, J. T. (1967). Esterase activities of human carbonic anhydrases B and C. *Journal of Biological Chemistry*, *242*(18), 4221–4229. https://doi.org/10.1016/S0021-9258(18)95800-X

Wu, Z., Shi, J., Chen, J., Hu, D., & Song, B. (2021). Design, synthesis, antibacterial activity, and mechanisms of novel 1, 3, 4-thiadiazole derivatives containing an amide moiety. *Journal of Agricultural and Food Chemistry*, *69*(31), 8660–8670. https://doi.org/10.1021/acs.jafc.1c01626

Yang, Y., Hu, X. Q., Li, Q. S., Zhang, X. X., Ruan, B. F., Xu, J., & Liao, C. (2016). Metalloprotein inhibitors for the treatment of human diseases. *Current Topics in Medicinal Chemistry*, *16*(4), 384–396. https://doi.org/10.2174/1568026615666150813145218